Near yrast study of the *fpg* shell nuclei ^{58}Ni, ^{61}Cu, and ^{61}Zn

S. M. Vincent,[1,*] P. H. Regan,[1] S. Mohammadi,[1,†] D. Blumenthal,[2] M. Carpenter,[2] C. N. Davids,[2] W. Gelletly,[1] S. S. Ghugre,[3] D. J. Henderson,[2] R. V. F. Janssens,[2] M. Hjorth-Jensen,[4] B. Kharraja,[5] C. J. Lister,[2] C. J. Pearson,[1] D. Seweryniak,[2] J. Schwartz,[2,6] J. Simpson,[7] and D. D. Warner[7]

[1]*Department of Physics, University of Surrey, Guildford GU2 5XH, United Kingdom*

[2]*Physics Division, Argonne National Laboratory, 9700 South Cass Avenue, Argonne, Illinois 60439*

[3]*IUCDAEF–Calcutta Centre, Calcutta 700 064, India*

[4]*Department of Physics, University of Oslo, P.O.B. 1048 Blindern, N-0316 Oslo, Norway*

[5]*Department of Physics, University of Notre Dame, Notre Dame, Indiana 46556*

[6]*A.W. Wright Nuclear Structure Laboratory, Yale University, New Haven, Connecticut 06511*

[7]*CLRC, Daresbury Laboratory, Daresbury, Warrington WA4 4AD, United Kingdom*

(Received 7 June 1999; published 10 November 1999)

The medium spin, near yrast states of the *fpg* shell nuclei ^{58}Ni, ^{61}Cu, and ^{61}Zn have been studied following the fusion evaporation of a ^{24}Mg beam and a ^{40}Ca target. Discrete transitions were unambiguously identified using the AYEBALL gamma-ray array in conjunction with the Argonne fragment mass analyzer and a split anode ionization chamber. The decay schemes of $^{58}_{28}$Ni, $^{61}_{29}$Cu, and $^{61}_{30}$Zn have been extended with the results of gamma-gamma coincidences and directional correlation from oriented state measurements used to determine the level excitation energies, spins, and parities of a number of near yrast states. The decay schemes deduced are compared with previous work and interpreted in terms of shell model calculations, with a restricted basis of the $f_{5/2}$, $p_{3/2}$, $p_{1/2}$ orbitals outside a $^{56}_{28}$Ni core, and either the $g_{9/2}$ orbital with a closed core, or $f_{7/2}$ excitations from the core. [S0556-2813(99)01112-7]

PACS number(s): 23.20.Lv, 21.60.Cs, 23.20.En, 27.40.+z

I. INTRODUCTION

The spectroscopy of doubly magic nuclei and their near immediate neighbors provides vital ingredients for the understanding of nuclear structure, as the single-particle energies and two-body residual interactions observed in these systems form the building blocks of large basis shell model calculations. Nuclei in the vicinity of self-conjugate, doubly magic nuclei are of particular interest since the protons and neutrons occupy the same orbitals giving rise to increased proton-neutron correlations. Much recent interest has focused on excited states in nuclei around the $N=Z=50$ shell gap at ^{100}Sn [1–5]. However, the very neutron deficient nature of these systems means that production cross sections for fusion-evaporation reactions are small and, as a result, only a few states can be identified. Of the four doubly magic, self-conjugate nuclei with $A>4$ ($^{16}_{8}$O, $^{40}_{20}$Ca, $^{56}_{28}$Ni, and $^{100}_{50}$Sn), high spin states are most accessible in nuclei near ^{56}Ni via fusion evaporation reactions induced by stable beams [6,7]. In addition, the nonyrast states in these nuclei can also be studied in beta-decay [8] and light-ion or neutron induced reaction studies [9–13]. As such, nuclei in this region provide an opportunity for a so-called ''complete'' spectroscopic study. Further information on high spin states in these nuclei will complement the information obtained in studies of nonyrast states, and allow us to build a full picture of the variety of excitation modes available in the rather restricted *fpg* single-particle basis between the $N=Z=28$ and 50 shell closures. In particular, it will allow us to examine how collective excitations are generated with increasing nucleon number away from the, nominally inert, ^{56}Ni core.

The mechanism for the generation of high angular momentum states in the restricted valence space around the ^{56}Ni core is of particular interest. Energetically speaking, the first three shell model orbitals above the $N=28$ closed shell are the negative parity $p_{3/2}$, $f_{5/2}$, and $p_{1/2}$ orbitals. The three lowest lying states in $^{57}_{28}$Ni all have negative parity and respective spins of $\frac{3}{2}^-$, $\frac{5}{2}^-$, and $\frac{1}{2}^-$, corresponding to a single neutron in these three shell model orbitals [14]. To generate a high spin value requires the breaking of the $N=Z=28$ core and/or the promotion of neutrons into the positive parity ''intruder'' $g_{9/2}$ orbital. These higher spin states are of particular interest for $A\sim60$ systems in light of both the theoretical predictions [15,16] and the recent experimental evidence [17,18] of a change at higher spins from a spherical to a highly collective, superdeformed prolate shape. The question of which mechanism is energetically preferred is one of the main motivations of this work. Other nuclear structure phenomena associated with collective excitations, including superdeformation [17], smooth band termination [18], and direct proton and alpha decay from deformed excited states [19] have also been recently reported for higher spin states in nuclei in this mass region.

Here, we present results of a near yrast study of the *fpg* shell systems ^{58}Ni, ^{61}Cu, and ^{61}Zn. In addition to the general interest in the build up of high spin configurations outlined above, a detailed and careful study of the medium spin, near yrast states in these nuclei is important for reliable as-

*Present address: Department of Physics, University of Notre Dame, Notre Dame, IN 46556.

†Permanent address: Physics Department, Payam-e-Nour University, Fariman 93914-33, Iran.

signments of spins and parities to states in superdeformed bands [17,18]. Also, the observation of direct proton decay from excited states in Cu nuclei [19,20] makes it important to determine the excitation energies, spins, and parities of the levels populated in the daughter (Ni) nuclei in order to provide a complete characterization of the proton-decaying state. Initial results of this study have been reported in a conference proceedings [21].

II. EXPERIMENTAL PROCEDURE AND DATA ANALYSIS

In order to first identify transitions and, subsequently, construct decay schemes of the nuclei under study in the current work, two separate experiments were performed at Argonne National Laboratory. The nuclei of interest were populated following the fusion-evaporation of a ^{24}Mg beam at an energy of 65 MeV, provided by the ATLAS accelerator, impinging on both a thin and thin backed ^{40}Ca target. In both experiments, gamma rays were detected using the AYEBALL detector array [22]. The array comprised both 20% efficient[1] TESSA type detectors [23,24] at angles of 79° and 101° with respect to the beam direction, and eight higher efficiency (70%) EUROGAM detectors [25] and one 70% GAMMASPHERE [26] prototype detector; four were placed at 134° and five at 158° with respect to the beam direction. The array had a measured photopeak efficiency of 1.1% at 1173 keV.

In the first experiment, the aim of which was to assign transitions unambiguously to a particular residual nucleus, the beam was incident on a target of natural calcium ($\sim$97% ^{40}Ca) of thickness 500 μg/cm^2 with a 300 μg/cm^2 Au coating facing the beam, and an additional 60 μg/cm^2 Au layer behind the calcium. Both layers served to reduce the oxidization of the calcium target. Isobaric identification of subsequent decay gamma rays was achieved by detecting the recoiling nuclei through the Argonne fragment mass analyzer (FMA) [27]. Elemental separation was provided by monitoring the recoil energy loss in a split-anode ionization chamber placed behind the focal plane of the FMA.

The second experiment was performed under the same beam conditions with a target of natural Ca of thickness 500 μg/cm^2, with a 300 μg/cm^2 Au coating facing the beam and a 20 mg/cm^2 Au backing, which was thick enough to stop the recoils in view of the array, thereby allowing high resolution γ-γ coincidence and angular correlation data to be collected.

A. Channel selection and generation of isotopically pure identification spectra

For a given charge state, the FMA disperses the residual nuclei according to their mass over charge (A/Q) ratio in the X direction at the focal plane, where they are detected by a position sensitive parallel grid avalanche counter (PGAC) [27]. As shown in Fig. 1, a two-dimensional (2D) spectrum of the position of the nuclei on the X axis of the PGAC versus the energy loss can be produced. By setting loci in the off-line analysis around the various A/Q contours of this two-dimensional plot, it was possible to generate gamma-ray spectra associated with particular A/Q values. These γ-ray spectra were often found to be contaminated by other, lighter masses due to the A/Q anomaly discussed below. However, as Fig. 2 shows, it was possible to subtract normalized amounts of contaminant channels from each spectrum to produce clean A/Q spectra.

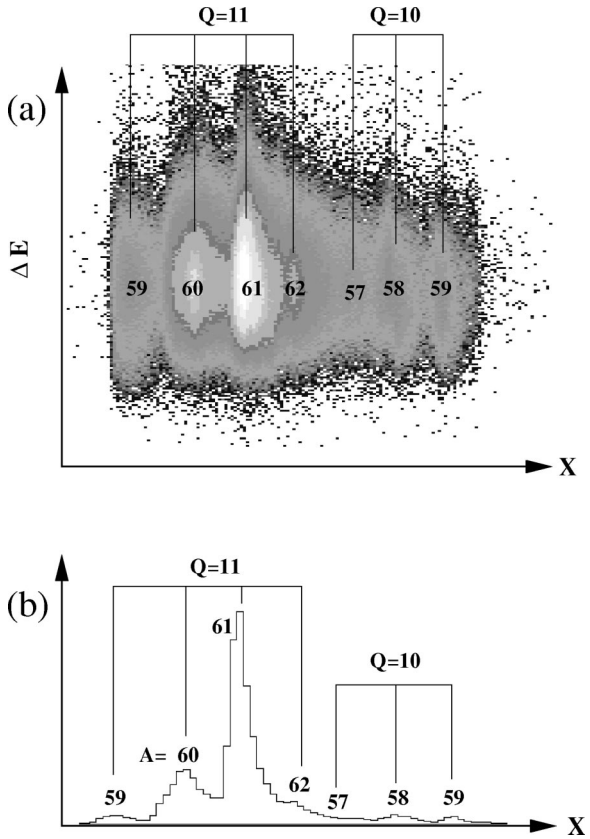

FIG. 1. (a) Recoil position X at the PGAC versus deposited energy; (b) projection on the X axis, showing the dispersion in the PGAC X direction of recoils in A/Q state ratio.

Note that for certain recoils, a charge state anomaly can cause an isobaric contamination in the A/Q gated spectra. The nominally $A=58$ gated spectrum shown in Fig. 2 also contains strong lines associated with decays in ^{64}Zn [28,29]. These arise from the strong $2p2n$ evaporation channel following reactions on the ^{44}Ca target contaminant. Note that the A/Q values for both $A=58$ and $A=64$ recoils are similar if their transmitted charge states differ by one, i.e., $\frac{58}{10} \approx \frac{64}{11}$. The contamination of these $A=64$ recoils was later removed by gating on the energy loss signal in the ion chamber (see Sec. II A 2).

1. Neutron detection

A ring of eleven NE213 scintillation detectors [30] was placed in front of the AYEBALL array, at the entrance of the FMA. These detectors were used to detect neutrons and subsequently select evaporation channels in the analysis, which

[1]Compared to a 3 in.$\times$3 in. crystal of sodium iodide [NaI(Tl)] at 25 cm for a 1.33 MeV γ-ray.

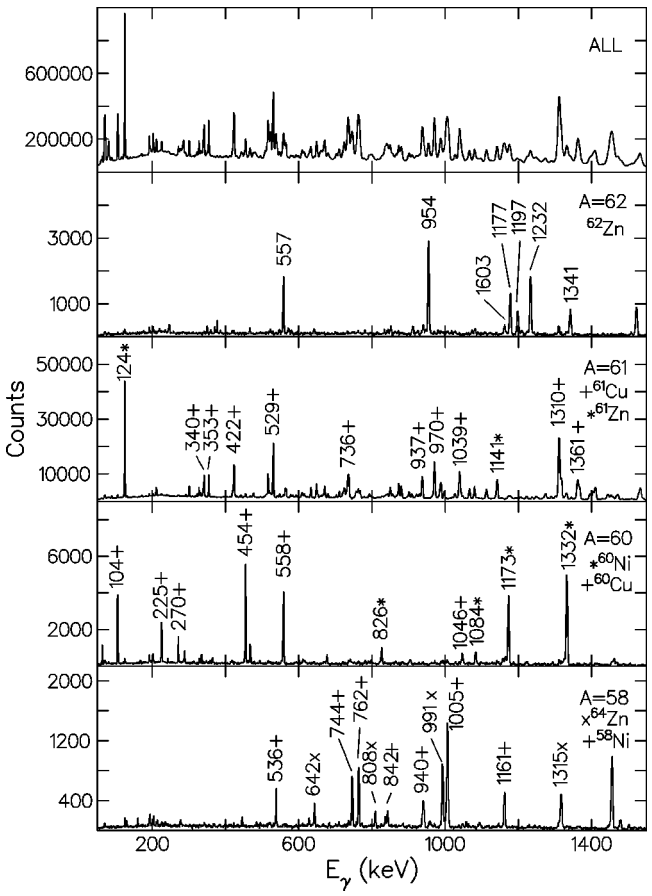

FIG. 2. Gamma-ray energy spectra gated by A/Q with normalized software subtractions of contaminants. The top spectrum, labeled ''All,'' is gated only by timing conditions and a recoil detection anywhere on the PGAC. The peaks marked with a plus, an *x*, or an asterisk are from the isotopic channel indicated to the left of the spectrum. ^{64}Zn is present from reactions on ^{44}Ca target contaminants and appears in the mass 58 spectrum due to an A/Q ambiguity ($\frac{58}{10} \simeq \frac{64}{11}$).

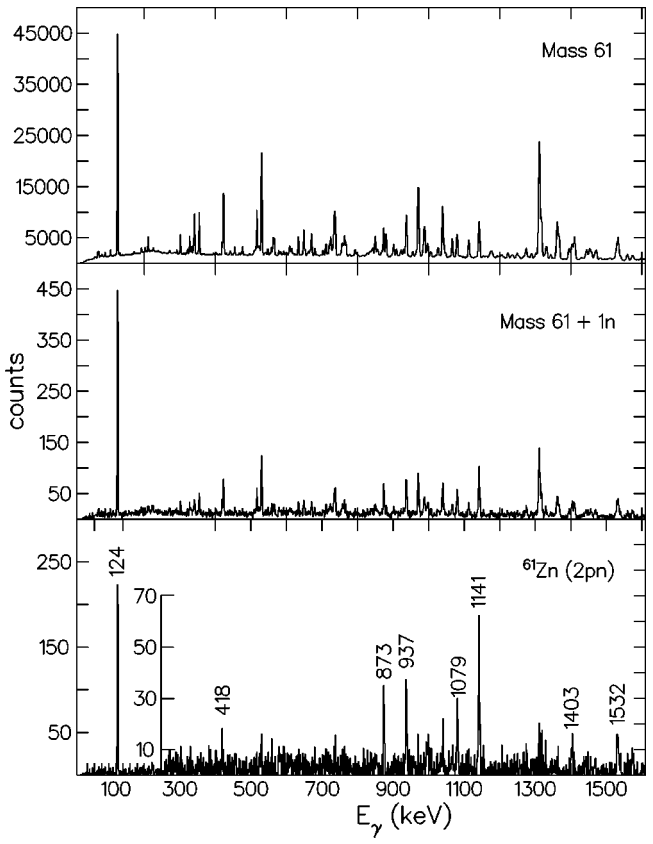

FIG. 3. Gamma-ray energy spectra gated on mass 61 (top), on mass 61, and one neutron (middle). The bottom spectrum shows the spectrum with the normalized amount of the top spectrum subtracted, thus showing a pure $2pn$ gated (^{61}Zn) identification spectrum.

involved one or more neutrons. Neutron/gamma-ray discrimination was achieved in these detectors in the off-line analysis by constructing two-dimensional spectra of both the time of flight versus total energy deposited in the detector, and the integrated slow component of the timing signal versus total energy. Examples of such 2D spectra can be found in Ref. [31]. In spite of this software gating, some γ rays were misidentified in the nominally ''pure-neutron'' gates. However, as Fig. 3 shows, the neutron evaporation channels could be clearly resolved by deconvoluting the spectra with and without the neutron condition. The neutron gating was able to resolve lines in the most strongly populated neutron evaporation channels. However, the measured neutron detection efficiency was rather low (measured from Fig. 3 using the intensity of the 124 keV peak in each spectrum to be $[I(61n)]/I(61) \approx 1\%$) and thus, in general, the ion chamber gating method was preferred to separate the isobarically gated spectra by an individual element (see the next subsection). The neutron detectors were used in conjunction with the ion chamber for the strongly populated channels as a method of confirming evidence in cases where ambiguities occurred.

2. Elemental separation using ionization chamber gating

A split anode ionization chamber was placed behind the focal plane of the FMA, which afforded a degree of elemental separation in proton number (Z). A plot of the total energy deposited in the ion chamber (E_{tot}), versus the sum of the energy measured at the first and second anodes (ΔE), was produced for all recoils. By setting software conditions in the off-line analysis on the recoil γ timing condition, and performing a normalized background subtraction of the random from the true events, the scattered beam component was effectively removed and, thus, the final peak to background in the gamma-ray identification spectra was improved significantly. This two-dimensional figure is shown in Ref. [31].

Figure 4 shows the projections of the plot, gated by transitions in ^{58}Ni and ^{64}Zn, showing the A/Q anomaly for these two recoils as discussed above. Gamma-ray spectra could then be produced, gated on either side of the ion chamber projection, and gated by A/Q. By deconvoluting these spectra and comparing the results with the neutron gated spectra, it was possible to produce data which were essentially isotopically pure. Figure 5 presents the spectra which have been isolated for ^{61}Cu ($3p$ channel) [32–35], ^{61}Zn ($2pn$)

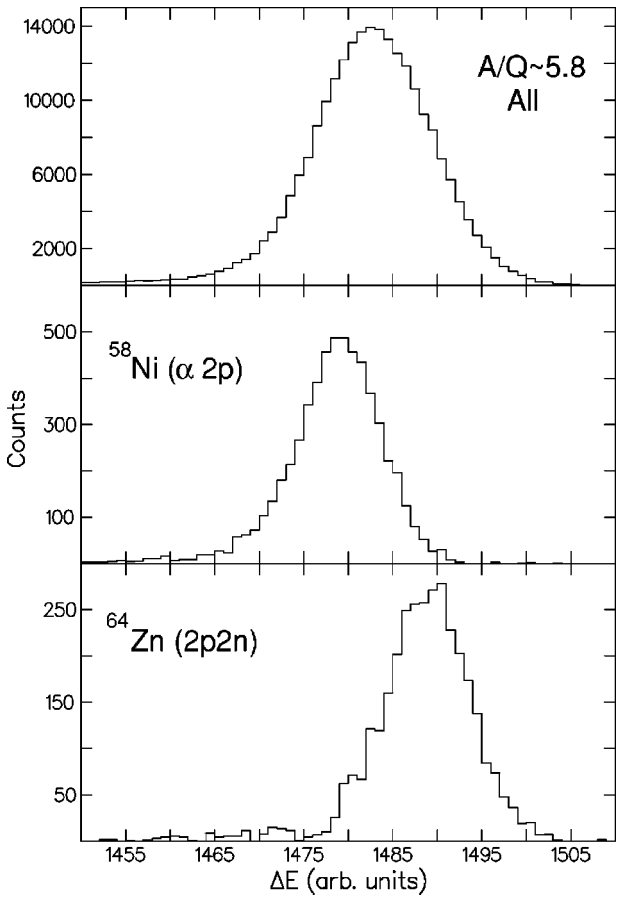

FIG. 4. Projections of the ion chamber signal gated by γ rays from two $A/Q \sim 5.8$ nuclei, ^{58}Ni $(Q=10)$, and ^{64}Zn $(Q=11)$.

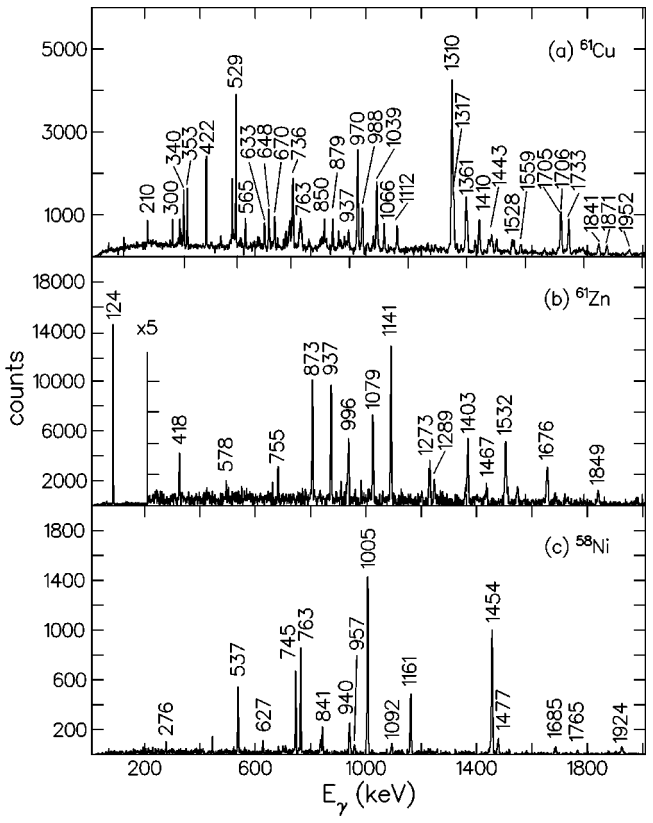

FIG. 5. Isotopically pure identification spectra for (a) ^{61}Cu, (b) ^{61}Zn, and (c) ^{58}Ni.

[22,36–38], and ^{58}Ni $(\alpha 2p)$ [39–41].

B. Backed target data

No Doppler broadening of line shapes could be observed for the low lying transitions in the backed target data. Therefore, these transitions appeared narrower in these spectra. These data were used to determine the coincidence relationships between the identified transitions in the nuclei of interest and to determine the multipolarity of the observed transitions.

1. Gamma-gamma coincidence analysis

Approximately 1.8×10^8 double and triple coincident gamma-ray events from the backed target data were unfolded into a γ-γ coincidence matrix. Coincidence gates were placed on this matrix for transitions identified in the thin target analysis described above. A selection of these backed targets, γ-γ coincidence spectra for gates on transitions identified in ^{58}Ni is shown in Fig. 6. Other spectra showing various other coincidence gates are given in Ref. [31].

2. Spin and parity assignments: DCO analysis

Multipolarities for transitions identified in each nucleus were assigned by using the *directional correlation from oriented states* (DCO) method [42–44] on pairs of γ rays detected in coincidence with one another. In this analysis, the detectors from the AYEBALL array were divided into two subsets; the detectors at angles 79°, 101°, and 134° were grouped together and sorted on one axis of a coincidence matrix, with coincident transitions detected at 158° placed on the other axis. By placing gamma-ray energy gates on transitions whose multipolarity had been established in previous works, a DCO ratio could be calibrated using the prescription outlined in Eq. (1):

$$R_{DCO}=\frac{I(158^\circ)\ \text{ gated at }\ (79^\circ,101^\circ,134^\circ)}{I(79^\circ,101^\circ,134^\circ)\ \text{ gated at }\ (158^\circ)}\times\varepsilon, \qquad (1)$$

where I is the number of counts in a peak and ε is an efficiency multiplication factor that corrects the experimental value for the detection efficiencies of both the gate and the projected transition. This factor is equal to

$$\varepsilon=\frac{\varepsilon_g(158^\circ)\times\varepsilon_p(79^\circ,101^\circ,134^\circ)}{\varepsilon_g(79^\circ,101^\circ,134^\circ)\times\varepsilon_p(158^\circ)}, \qquad (2)$$

where ε_g is the detection efficiency of the gate and ε_p is the detection efficiency of the projected transition. A similar analysis has been carried out for the pn evaporation channel leading to ^{62}Ga, and is described in Ref. [45]. The difference in the projected intensity of stretched quadrupole γ rays (assumed to be of $E2$ character) and $\Delta I=1$ transitions, when both are gated by an $E2$ transition, is clearly illustrated for ^{61}Cu in Fig. 7. This spectrum is gated by the strongly popu-

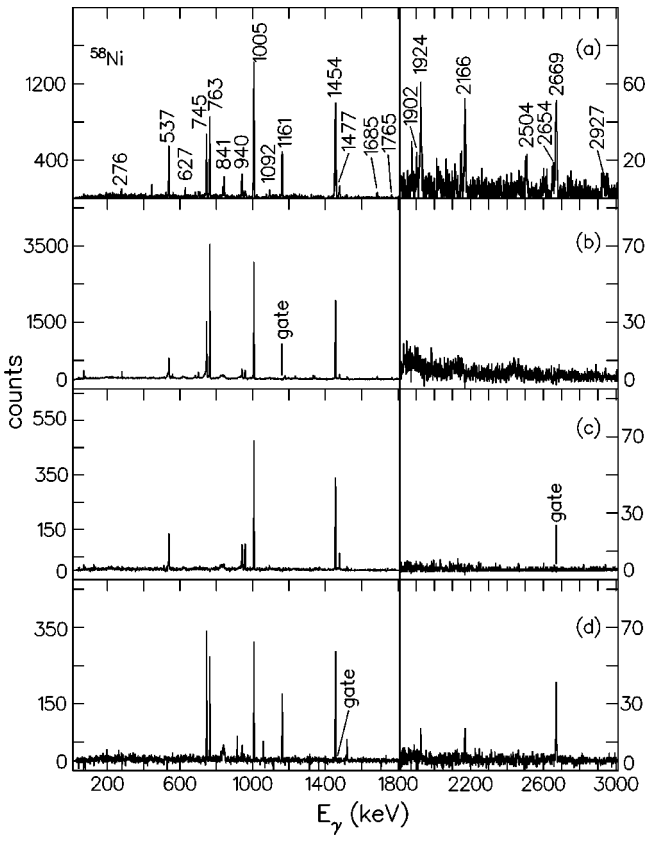

FIG. 6. Gamma-gamma coincidence spectra for ^{58}Ni from the backed target experiment. The clean mass and ion-chamber gated id-spectrum for this nucleus is also shown for comparison (a). The spectra are gated by transitions of (b) 1161 keV, (c) 2669 keV, and (d) 1477 keV, respectively.

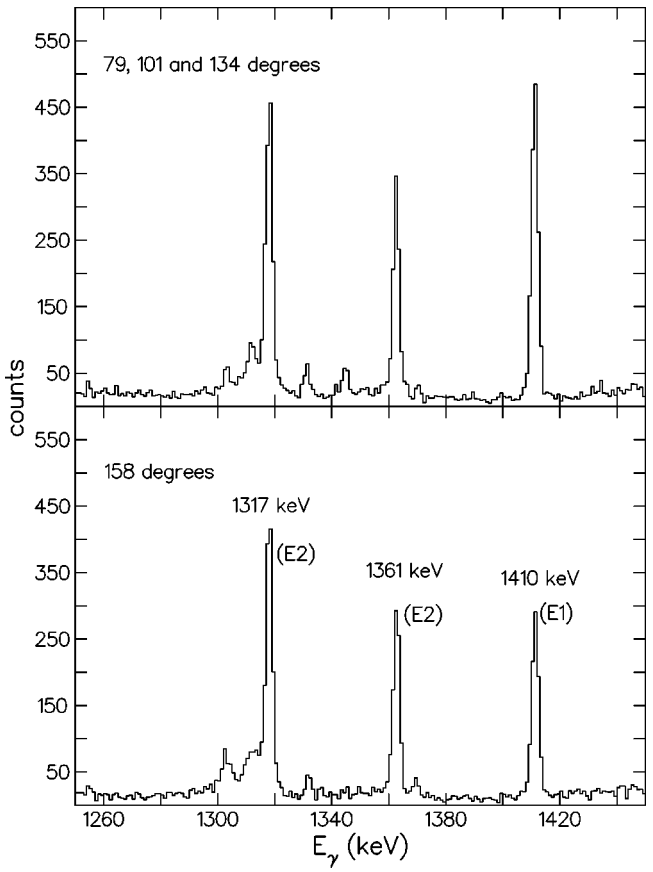

FIG. 7. DCO ^{61}Cu gated spectra (gated by 1310 keV $\frac{7}{2}^- \rightarrow \frac{3}{2}^-$ pure $E2$) highlighting the difference in the angle gated spectra, for $\Delta I=2$ and $\Delta I=1$ transitions.

lated 1310 keV, $\frac{7}{2}^- \rightarrow \frac{3}{2}^-$ (stretched $E2$) transition previously reported in this nucleus [33]. The 1317 keV, $\frac{11}{2}^- \rightarrow \frac{7}{2}^-$ and 1361 keV, $\frac{13}{2}^+ \rightarrow \frac{9}{2}^+$ $E2$ transitions [33] shown in the figure are of roughly equal intensity in both projections, while the 1410 keV, $\frac{9}{2}^+ \rightarrow \frac{7}{2}^-$ $E1$ transition [33] is clearly more intense in the summed spectrum of detectors nearer 90°. Since, for transitions from higher spin states, there was often a Doppler shifted component to the peaks, associated with the feeding of these levels by fast statistical transitions prior to the recoils stopping in the target backing, special care was taken in determining the intensity of these transitions for the DCO analysis [46]. Figure 8 shows this effect for the 1705 keV, $(\frac{21}{2}^+) \rightarrow \frac{17}{2}^+$ transition in ^{61}Cu for the two angular projections, with the maximum shift calculated and labeled at 1694 keV for 101°, 1671 keV for 134°, and 1660 keV for 158°. The 1733 keV transition decaying from a lower lying state is shown for comparison and shows no shifted component.

The measured DCO ratios for the strongly populated levels, gated by stretched quadrupole transitions in ^{58}Ni, and by both dipole and stretched quadrupole transitions in ^{61}Cu and ^{61}Zn, are plotted in Fig. 9. The gating dipole γ rays are chosen to be as pure as possible, being either of an electric dipole nature (where any $M2$ admixture is assumed to be negligible), or of an $M1$ character with very little $E2$ admixture. A clear separation is apparent between transitions of different multipolarities. An analysis of the weighted averaged values for transitions of known multipolarity yielded typical values of the DCO ratio of 0.95(3) and 0.62(2) for stretched quadrupole and pure dipole transitions, respectively, when gated by a stretched $E2$ transition [45]. Alternatively, for a pure dipole ($\Delta I=1$) gate, the weighted average of extracted DCO ratios for previously identified transitions was found to be 1.60(3) and 0.92(6) for stretched quadrupole and pure dipole transitions, respectively. Ratios for all γ rays observed with sufficient statistics are given for ^{61}Cu, ^{61}Zn and ^{58}Ni in Tables I, II, and III, respectively. The gating transitions, indicated in the tables, are always chosen to be $E2$ for ease of comparison.

The spin assignments have been made on the basis of the measured DCO values by restricting the possible multipolarities to $E2$ or $\Delta I=1$, $E1$ or mixed $M1/E2$ type decays. The usual assumption that heavy-ion fusion-evaporation reactions preferentially populate near-yrast states has also been applied [47] and, thus, the spins generally increase with increasing excitation energy. Note that in the present analysis, transitions that lie between the values for a pure dipole and a stretched quadrupole are usually assumed to be of a mixed $M1/E2$ character. $\Delta I=0$, $J \rightarrow J$ type transitions cannot be determined unequivocally from the DCO analysis, however, in certain cases such decays can be inferred by applying consistency arguments to the decay scheme, primarily by

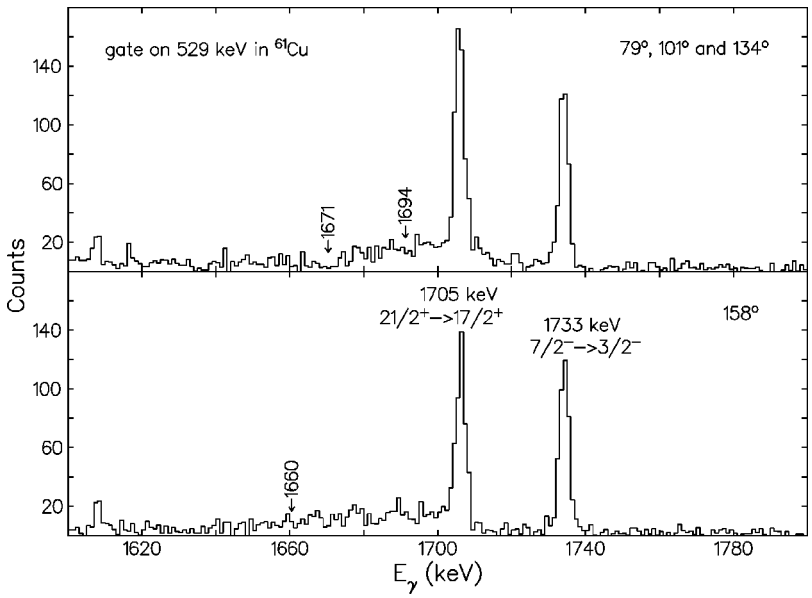

FIG. 8. DCO gated spectra (gated by 529 keV $\frac{17}{2}^+ \rightarrow \frac{13}{2}^+$ pure $E2$) for transitions in ^{61}Cu, showing 1705 keV, $(\frac{21}{2}^+) \rightarrow \frac{17}{2}^+$ transition with shifted components labeled at 1694 keV for 101°, 1671 keV for 134°, and 1660 keV for 158°. The 1733 keV $\frac{7}{2}^- \rightarrow \frac{3}{2}^-$ transition in contrast has no shifted component.

analyzing different decay routes from the same initial excited state.

III. DISCUSSION OF DECAY SCHEMES

The decay schemes for ^{61}Cu, ^{61}Zn, and ^{58}Ni deduced from this work are shown in Figs. 10–12, respectively. Spin and parity assignments, taken from DCO ratios using a stretched $E2$ as the gating transition, along with gamma-ray intensities, measured in the mass gated singles data, are tabulated in Tables I–III, respectively. The intensities are indicated in Figs. 10–12 by the widths of the arrows. Spin and/or parity labels in brackets indicate tentative assignments.

A. ^{61}Cu

Prior to this study, near yrast states had been observed in the nucleus ^{61}Cu up to an excitation energy of 4081 keV and a tentative spin of $\frac{13}{2}^+$, using the light-ion reactions ^{58}Ni$(\alpha,p\gamma)^{61}$Cu [33,34] and ^{60}Ni$(p,\gamma)^{61}$Cu [48,49], the heavy-ion fusion-evaporation reaction ^{40}Ca$(^{24}$Mg,3$p)^{61}$Cu [35], and the stripping reaction ^{60}Ni$(^3$He,$d)^{61}$Cu [50]. This work extends the near yrast data by 16 new levels up to an excitation energy of 9408 keV, and determines the spins and parities of the previously observed levels at 2627, 3016, 3260, 3548, 3942, and 4081 keV.

All the near yrast energy level assignments made in previous works are in agreement with the present data. As examples of the effectiveness of the DCO method for determining multipolarity, the measured DCO ratios of three intense transitions in this data, namely, 1310, 1410, and 970 keV, are 1.10 ± 0.04,0.56 ± 0.05, and 0.45 ± 0.03 when gated by an $E2$ transition, respectively. The multipolarity assignments can thus be made a stretched $E2$ for the 1310 keV ($\frac{7}{2}^- \rightarrow \frac{3}{2}^-$) γ ray, as an $E1$ dipole transition for the 1410 keV line ($\frac{9}{2}^+ \rightarrow \frac{7}{2}^-$), and as a mixed $M1/E2$ transition for the 970 keV γ ray ($\frac{5}{2}^- \rightarrow \frac{3}{2}^-$). All of these assignments are in agreement with those proposed by Sarantites *et al.* [34], Sziklai *et al.* [48], and Tingwell *et al.* [49]. Similarly, when gated by the 1410 keV $E1$ transition, the DCO ratios for the 340 keV and the 1310 keV transitions are 0.94 ± 0.14 and 1.64 ± 0.04, respectively, consistent with the $M1/E2$ and stretched $E2$ assignments previously reported [34,48,49].

Many of the nonyrast states previously identified in the references cited above are not observed in our data. The ^{60}Ni$(p,\gamma)^{61}$Cu study by Sziklai *et al.* [48] identified a number of nonyrast states up to an excitation energy of $\sim$4 MeV, which are not identified in our data. Such states include a $\frac{7}{2}^-$ level at 2399 keV and a $\frac{9}{2}^+$ state at 4132 keV. The light-ion induced reaction reported by Tingwell *et al.* [49] also identifies nonyrast decays which are not observed in the current data set, namely, low lying $\frac{1}{2}^-$ states at excitation energies of 475 keV and 2089 keV, two $\frac{3}{2}^-$ states at 1660 keV and 1933 keV, and two nonyrast $\frac{5}{2}^-$ levels at 1394 keV and 1904 keV. The fact that these nonyrast states are not observed here, presumably due to their weak population in this heavy-ion fusion-evaporation reaction, supports the assumption of near yrast population used for the spin assignments of the higher lying states.

During the analysis of this work, a high-spin study of this nucleus was published by Hatsukawa *et al.* [32] using the reaction ^{40}Ca$(^{28}$Si,$\alpha 3p)^{61}$Cu, producing a decay scheme which is, in general, consistent with our data. Their study identified all but the 210, 326, 353, 565, 909, and 1975 keV transitions (see Fig. 10), with one contradiction to our gamma decay ordering (outlined below), although many levels were not assigned a spin or a parity. The new assignments made in this study are now discussed individually.

The spin and parity assignments shown in Fig. 10 were made assuming a $I^\pi = \frac{3}{2}^-$ ground state. These quantum numbers were derived based on the beta decay study by Singh *et al.* [51].

(i) 1942 keV level. There was a decay observed from this state to the $\frac{7}{2}^-$ 1732 keV level, with an energy of 209.6(2) keV. This decay was not seen in any previous work, includ-

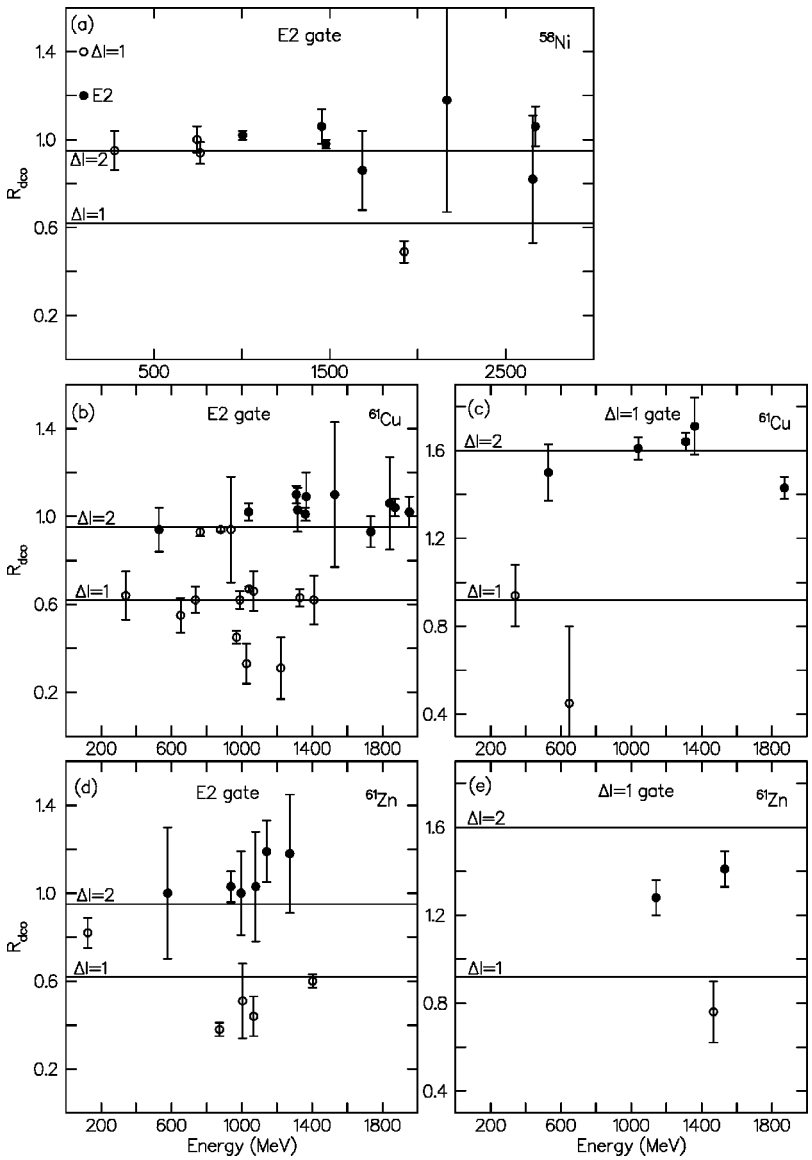

FIG. 9. DCO ratios for (a) ^{58}Ni gated by an $E2$; for ^{61}Cu gated by (b) an $E2$ and (c) a pure dipole γ ray; for ^{61}Zn gated by (d) an $E2$ and (e) a pure dipole transition. Weighted averages of previously known transitions are indicated by the horizontal lines.

ing that of the Hatsukawa group [32]. The DCO ratio of this transition was measured to be 0.78(10), and the ratio of the 670 keV transition from the $\frac{9}{2}^-$ state at 2612 keV was measured as 0.95(12). The 972 keV transition to the $\frac{5}{2}^-$ level was contaminated by the 970 keV transition to the ground state in all possible DCO gates, allowing for no clean ratio to be obtained. These ratios are insufficient to assign a multipolarity, however, the spins and parities of the states feeding into and out of this state, suggest probable assignments for the 1942 keV level of either $\frac{9}{2}$ or $\frac{7}{2}$, with negative parity. Given that this state would constitute a yrast $\frac{9}{2}$ level, and the relatively weak population intensity, an assignment of $\frac{7}{2}^-$ has been tentatively given.

(ii) 2336 keV level. A link between this level and a band built on the ground state was observed in the study by Hatsukawa *et al.* [32], although no such band or link were observed in this data.

(iii) 2627 keV level. The spin and parity of this level is assigned $\frac{11}{2}^-$ on the basis of the DCO ratio of 1.03(10) measured for the 1317 keV transition to the $I^\pi=\frac{7}{2}^-$ level at 1310 keV, suggesting a stretched $E2$ transition. This assignment is also favored over one of $\frac{9}{2}$ as the level is strongly populated, suggesting it is yrast.

(iv) 3016 keV level. The spin and parity of this level has been assigned $\frac{11}{2}^-$ on the basis of the DCO measurement of the feeding 1066 keV transition from the $\frac{13}{2}^+$ level at 4081 keV. The ratio of 0.66(9) is indicative of a pure electric dipole transition.

(v) 3260 keV level. The 1528 keV transition to the $\frac{7}{2}^-$ state has a DCO ratio of 1.10(33), which is uncertain, but allows for a possible assignment of $\frac{7}{2}, \frac{9}{2}$, or $\frac{11}{2}$. The DCO ratio of the 633 keV transition depopulating this state can give no indication as to whether or not it is a $J \rightarrow J$ transition since the DCO method in insensitive to these types of decays. Also the ratio of the 648 keV transition cannot be determined due to the doublet at higher excitation energy. However, since population of near yrast states is favored in this type of reaction, and the state decays to the $\frac{11}{2}^-$ state discussed above, an assignment of $\frac{11}{2}$ is most likely, although the parity has not been assumed.

TABLE I. Transitions identified in ^{61}Cu in the present work. The number in the DCO gate column refers to the $E2$ gating transition used in the DCO analysis, labeled with a number in square brackets in the last column. Transitions with their energies labeled in bold type were identified in previous studies of this nucleus [33,34]. Intensities are relative to the 1310 keV $\frac{7}{2}^- \rightarrow \frac{3}{2}^-$ transition [33].

E_γ (keV)	Intensity singles (%)	Intensity γ-γ (%)	E_i (keV)	E_f (keV)	I_i	I_f	RDCO	DCO gate
209.6 (2)	2.6 (1)	2.0 (1)	1942	1732	$(\frac{7}{2}^-)$	$\frac{7}{2}^-$	0.78 (10)	1
300.2 (3)	1.8 (1)	2.3 (1)	5120	4820	$\frac{17}{2}^+$	$(\frac{15}{2}^-)$	0.62 (13)	2
326.4 (4)	2.5 (4)	0.5 (1)	5465	5138		$(\frac{15}{2}^+)$	0.65 (35)	5
340.2 (2)	7.5 (5)	18.1 (3)	1310	970	$\frac{7}{2}^-$	$\frac{5}{2}^-$	0.64 (11)	3
352.9 (5)	7.2 (0.5)	1.3 (1)	6056	5703	$(\frac{17}{2}^+)$	$(\frac{15}{2}^+)$	0.49 (11)	2
422.0 (1)	13.6 (13)	23.2 (9)	1732	1310	$\frac{7}{2}^-$	$\frac{7}{2}^-$	1.16 (12)	2
529.3 (1)	23.7 (15)	27.5 (9)	5120	4590	$\frac{17}{2}^+$	$\frac{13}{2}^+$	0.94 (10)	2 [1]
564.6 (2)	4.0 (38)	1.1 (1)	5703	5138	$(\frac{15}{2}^+)$	$(\frac{15}{2}^+)$	0.75 (42)	5
632.7 (9)	6.2 (7)	5.4 (3)	3260	2627	$(\frac{11}{2})$	$\frac{11}{2}^-$	1.02 (9)	1
647.5 (5)	2.1 (3)	1.0 (1)	4590	3942	$\frac{13}{2}^+$	$\frac{11}{2}^+$		
648.2 (1)	8.9 (3)	5.4 (2)	3260	2612	$(\frac{11}{2})$	$\frac{9}{2}^-$		
651.6 (3)	1.7 (1)	2.3 (1)	5120	4468	$\frac{17}{2}^+$	$\frac{15}{2}^-$	0.55 (8)	3
669.5 (3)	8.6 (13)	3.7 (2)	2612	1942	$\frac{9}{2}^-$	$(\frac{7}{2}^-)$	0.95 (12)	1
735.9 (1)	26.1 (22)	14.6 (5)	5856	5120	$\frac{19}{2}(-)$	$\frac{17}{2}^+$	0.56 (3)	1
762.5 (1)	7.8 (49)	10.9 (5)	1732	970	$\frac{7}{2}^-$	$\frac{5}{2}^-$	0.93 (2)	1
849.7 (2)	8.5 (9)	3.2 (2)	5138	4288	$(\frac{15}{2}^+)$	$\frac{13}{2}^-$	0.63 (10)	5
879.2 (2)	8.9 (15)	10.5 (5)	2612	1732	$\frac{9}{2}^-$	$\frac{7}{2}^-$	0.94 (1)	1
908.5 (2)	2.6 (2)	3.2 (2)	4990	4081	$(\frac{15}{2}^+)$	$\frac{13}{2}^+$	0.30 (1)	8
936.5 (3)	19.0 (13)	4.2 (3)	3548	2612	$\frac{11}{2}(-)$	$\frac{9}{2}^-$	0.94 (24)	1
969.9 (1)	36.7 (7)		970	0	$\frac{5}{2}^-$	$\frac{3}{2}^-$	0.45 (3)	5
972		7.1 (4)	1942	970	$(\frac{7}{2}^-)$	$\frac{5}{2}^-$		
987.5 (3)	19.8 (7)	22.1 (8)	2720	1732	$\frac{9}{2}^+$	$\frac{7}{2}^-$	0.61 (5)	6
1026.3 (5)	4.5 (8)	5.5 (3)	2336	1310	$\frac{9}{2}^-$	$\frac{7}{2}^-$	0.33 (9)	2
1038.5 (2)	24.8 (8)	37.7 (11)	5120	4081	$\frac{17}{2}^+$	$\frac{13}{2}^+$	1.02 (4)	4
1041.9(2)	12.0 (13)	3.6 (2)	4590	3548	$\frac{13}{2}^+$	$\frac{11}{2}(-)$	0.67 (1)	1
1065.5(4)	10.8 (6)	10.0 (4)	4081	3016	$\frac{13}{2}^+$	$\frac{11}{2}^-$	0.66 (9)	2
1112.2(3)	11.1 (8)	9.3 (4)	7937	6825		$(\frac{21}{2}^+)$	0.82 (15)	1
1222.2 (1)	4.0 (5)	3.3 (3)	3942	2720	$\frac{11}{2}^+$	$\frac{9}{2}^+$	0.46 (11)	1
1310.4 (1)	100.0 (55)	100.0 (54)	1310	0	$\frac{7}{2}^-$	$\frac{3}{2}^-$	1.10 (4)	4 [2]
1316.9 (1)	23.4 (35)	37.8 (15)	2627	1310	$\frac{11}{2}^-$	$\frac{7}{2}^-$	1.03 (10)	1 [3]
1330.0 (1)	11.6 (19)	6.3 (3)	4590	3260	$\frac{13}{2}^+$	$(\frac{11}{2})$	0.63 (4)	1
1361.0 (1)	35.9 (21)	36.2 (13)	4081	2720	$\frac{13}{2}^+$	$\frac{9}{2}^+$	0.94 (12)	2 [4]
1366.2 (1)	14.7 (21)	17.9 (8)	2336	970	$\frac{9}{2}^-$	$\frac{5}{2}^-$	1.09 (11)	7 [5]
1409.7 (1)	20.8 (14)	32.5 (12)	2720	1310	$\frac{9}{2}^+$	$\frac{7}{2}^-$	0.56 (5)	4
1443.2 (2)	11.8 (34)	4.1 (3)	3780	2336	$(\frac{11}{2}^-)$	$\frac{9}{2}^-$		
1471.4 (3)	7.1 (16)	4.2 (2)	9408	7937				
1528.1 (1)	17.2 (36)	7.9 (4)	3260	1732	$(\frac{11}{2})$	$\frac{7}{2}^-$	1.10 (33)	6
1533.0 (1)	3.2 (2)	2.6 (2)	7389	5856		$\frac{19}{2}(-)$	0.50 (14)	8
1559.4 (2)	6.0 (4)	2.4 (2)	4820	3260	$(\frac{15}{2}^-)$	$(\frac{11}{2})$	1.50 (12)	6
1704.9 (1)	11.1 (10)	16.0 (6)	6825	5120	$(\frac{21}{2}^+)$	$\frac{17}{2}^+$	1.18 (3)	1
1706(1)	23.6 (21)	15.0 (10)	3016	1310	$\frac{11}{2}^-$	$\frac{7}{2}^-$		
1732.5 (1)	28.0 (16)	36.7 (17)	1732	0	$\frac{7}{2}^-$	$\frac{3}{2}^-$	0.93 (7)	4 [6]
1841.3 (1)	12.9 (10)	4.1 (3)	4468	2627	$\frac{15}{2}^-$	$\frac{11}{2}^-$	1.06 (21)	3
1870.5 (2)	9.4 (3)	11.4 (5)	4590	2720	$\frac{13}{2}^+$	$\frac{9}{2}^+$	1.04 (4)	2
1952.0 (1)	4.8 (2)	4.2 (3)	4288	2336	$\frac{13}{2}^-$	$\frac{9}{2}^-$	1.02 (7)	5 [7]
1975 (1)	1.8 (4)	0.5 (1)	6056	4081	$(\frac{17}{2}^+)$	$\frac{13}{2}^+$		
2193.6 (2)	4.4 (8)	0.7 (1)	4820	2627	$(\frac{15}{2}^-)$	$\frac{11}{2}^-$	0.64 (39)	3

TABLE II. Transitions identified in ^{61}Zn in the present work. The number in the DCO gate column refers to the $E2$ gating transition used in the DCO analysis, labeled with a number in square brackets in the last column. Transitions with their energies labeled in bold type were identified prior to this study [36]. Intensities are relative to the 124 keV $\frac{5}{2}^- \rightarrow \frac{3}{2}^-$ transition [36].

E_γ (keV)	Intensity singles (%)	Intensity γ-γ (%)	E_i (keV)	E_f (keV)	I_i	I_f	RdCO	DCO gate
123.9 (1)	100.0 (19)		124	0	$\frac{5}{2}^-$	$\frac{3}{2}^-$	0.82 (7)	1
418.4 (1)	7.8 (5)		418	0	$\frac{3}{2}^-$	$\frac{3}{2}^-$	0.89 (23)	2
578.0 (2)	5.3 (6)	2.9 (9)	996	418	$\frac{7}{2}^-$	$\frac{3}{2}^-$	0.85 (23)	1
872.7 (4)	43.5 (83)	37.7 (14)	996	124	$\frac{7}{2}^-$	$\frac{5}{2}^-$	0.38 (3)	1
936.6 (3)	56.9 (49)	37.5 (14)	3336	2400	$\frac{13}{2}^-$	$\frac{9}{2}^-$	1.03 (7)	2 [1]
996.2 (2)	27.4 (28)	23.1 (12)	996	0	$\frac{7}{2}^-$	$\frac{3}{2}^-$	1.00 (19)	1
1005.4(3)	2.8 (6)	4.3 (3)	2270	1265	$\frac{11}{2}^-$	$\frac{9}{2}^-$	0.51 (17)	3
1019.4 (2)	5.0 (19)	1.2 (1)	4264	3246	$(\frac{15}{2})$	$(\frac{13}{2}^-)$		
1066.6 (4)	12.5 (23)	5.0 (3)	3336	2270	$\frac{13}{2}^-$	$\frac{11}{2}^-$	0.44 (9)	2
1078.9 (2)	49.8 (19)	30.0 (11)	4415	3336	$\frac{17}{2}^-$	$\frac{13}{2}^-$	1.03 (25)	1 [2]
1141.3 (1)	90.6 (41)	61.3 (22)	1265	124	$\frac{9}{2}^-$	$\frac{5}{2}^-$	1.19 (14)	1 [3]
1273.0 (5)	34.5 (51)	12.8 (7)	2270	996	$\frac{11}{2}^-$	$\frac{7}{2}^-$	1.25 (33)	2
1288.7 (3)	12.2 (32)	6.3 (3)	5553	4264	$(\frac{19}{2})$	$(\frac{15}{2})$	1.04 (18)	3
1396.9 (4)	38.6 (23)	2.7 (2)	7488	6091		$(\frac{21}{2}^-)$	0.71 (27)	2
1403.3 (2)	64.3 (74)	36.3 (18)	2400	996	$\frac{9}{2}^-$	$\frac{7}{2}^-$	0.60 (3)	1
1466.7 (3)	27.5 (58)	7.0 (4)	4264	2797	$(\frac{15}{2})$	$(\frac{13}{2}^-)$	0.36 (10)	3
1532.2 (1)	54.1 (63)	20.6 (9)	2797	1265	$(\frac{13}{2}^-)$	$\frac{9}{2}^-$	1.26 (17)	3
1533.1 (4)	4.3 (9)	3.3 (3)	9163	7630			0.72 (44)	2
1538.9 (3)	10.0 (26)	4.5 (3)	7630	6091		$(\frac{21}{2}^-)$	0.68 (23)	2
1675.5 (1)	52.5 (71)	8.5 (4)	6091	4415	$(\frac{21}{2}^-)$	$\frac{17}{2}^-$	1.15 (46)	1
1849 (1)	8.3 (26)	2.4 (2)	4646	2797	$(\frac{17}{2}^-)$	$(\frac{13}{2}^-)$	1.05 (38)	3
1980.5 (5)	9.7 (6)	1.4 (2)	3246	1265	$(\frac{13}{2}^-)$	$\frac{9}{2}^-$	0.77 (46)	3
2276.1 (3)	7.3 (12)	1.0 (2)	2400	124	$\frac{9}{2}^-$	$\frac{5}{2}^-$	1.61 (69)	2

(vi) 3548 keV level. The work published by Hatsukawa *et al.* [32] places the 937 keV and the 1042 keV transitions between the 4590 keV $\frac{13}{2}^+$ and 2612 keV $\frac{9}{2}^-$ states in the opposite order to the one shown in Fig. 10. This is contrary to the intensities measured from this data set, given in Table I. The spin of the level is determined by the DCO ratios of these two transitions, both being of dipole nature. The parity is assigned as negative since the 1042 keV transition has a ratio of 0.67(1), being consistent with an $E1$. However, an $M1$ cannot be ruled out, so the assignment is left tentative.

(vii) 3780 keV level. There is a 1443 keV transition identified in coincidence with the 1366 keV gamma ray, which is not present is the 1952 keV gate. The transition is therefore placed in a parallel branch feeding the same level. The DCO ratio is undetermined, however, if it were an $E2$, then the 3780 keV level would be $\frac{13}{2}$, making it yrast, which is not consistent with its observed intensity. The transition is therefore tentatively assigned as an $M1/E2$.

(viii) 3942 keV level. The DCO ratio of the 1222 keV transition to the $\frac{9}{2}^+$ 2720 keV level is 0.46(11), indicative of a mixed dipole, thus making the state an $\frac{11}{2}^+$.

(ix) 4081 keV level. This level is consistent with being yrast; it has a depopulating decay which is consistent with an $E2$; and is therefore assigned as a $\frac{13}{2}^+$.

(x) 4288 keV level. The 1952 keV transition feeding into the 2336 keV level has a DCO ratio of 1.02(7), and is considered to be an $E2$, giving the feeding level a spin/parity of $\frac{13}{2}^-$.

(xi) 4468 keV level. The DCO ratio of the 1841 keV transition depopulating this level into an $\frac{11}{2}^-$ level is consistent with an $E2$ and, moreover, the DCO ratio of the 652 keV transition feeding this state from a $\frac{17}{2}^+$ state is indicative of an $E1$. Therefore, the state is $\frac{15}{2}^-$. This also helps to tie in the assignment given to the 2627 keV level, which it feeds.

(xii) 4590 keV level. An $E2$ multipolarity assignment for the 1871 keV transition from the DCO ratio of 1.04(4) gives this level a spin/parity of $\frac{13}{2}^+$.

(xiii) 4820 keV level. The spin and parity of this level could not be determined with confidence from this data set, however, assignments of $\frac{13}{2}$ or $\frac{15}{2}$ are favored due to the spin change between the feeding states above and below this level. The 0.62(13) ratio of the 300 keV transition from the $\frac{17}{2}^+$ 5120 keV state is suggestive of a parity changing dipole, so the state is tentatively assigned $\frac{15}{2}^-$ quantum numbers.

(xiv) 4990 keV level. There is a 909 keV transition feeding the 4081 keV, yrast $\frac{13}{2}^+$ state, which is not observed in the

TABLE III. Transitions identified in ^{58}Ni in the present work. The DCO numbers are all from spectra gated by the sum of the 1454 keV $2^+ \rightarrow 0^+$ and 1005 keV $4^+ \rightarrow 2^+$ transitions. Transitions with their energies labeled in bold type were known prior to this study [39]. Intensities are relative to the 1005 keV $4^+ \rightarrow 2^+$ transition [39].

E_γ (keV)	Intensity singles (%)	Intensity γ-γ (%)	E_i (keV)	E_f (keV)	I_i	I_f	RDCO
275.6 (4)	3 (1)	3 (1)	4383	4108	5^+	4	0.95(9)
536.7 (3)	14 (1)	15 (1)	6605	6068	8^+	(7^+)	
626.8 (5)	3 (1)	4 (1)	7232	6605			
682.4 (5)	1 (1)	2 (1)	6068	5386	(7^+)	(5,6)	0.32(8)
698.8 (5)	2 (1)	2 (1)	6085	5386	(6)	(5,6)	0.46(8)
708.0 (5)	1 (1)	2 (1)					
744.6 (3)	30 (3)	27 (4)	5128	4383	6^+	5^+	1.00(6)
762.9 (3)	35 (2)	35 (2)	4383	3620	5^+	4^+	0.94(5)
834.6 (4)	7 (1)						
841.3 (4)	11 (1)		7446	6605	(10)	8^+	0.99(9)
940.1 (4)	19 (2)	16 (2)	6068	5128	(7^+)	6^+	
956.9 (7)	5 (1)	4 (1)	6085	5128	(6)	6^+	0.86(16)
1002.0 (10)			5386	4383	(5,6)	4^+	0.94(6)
1004.9 (5)	100 (4)	100 (2)	2459	1454	4^+	2^+	1.02(2)
1092.4 (5)	6 (1)	8 (2)	6220	5128	(7)	6^+	0.67(23)
1161.1 (3)	39 (5)	42 (4)	3620	2459	4^+	4^+	1.10(10)
1256.2 (5)	2 (1)						0.30(12)
1454.4 (4)	122 (7)		1454	0	2^+	0^+	1.06(8)
1476.8 (11)	14 (2)	14 (4)	6605	5128	8^+	6^+	0.98(2)
1516.5 (7)	5 (2)	3 (2)	8121	6605	(9)	8^+	0.61(12)
1684.7 (10)	8 (2)	8 (2)	6068	4383	(7^+)	5^+	0.86(18)
1764.8 (11)	5 (2)	3 (1)	5386	3620	(5,6)	4^+	0.50(16)
1901.7 (12)	3 (1)		4361	2459	(5)	4^+	
1924.0 (7)	13 (2)	11 (3)	4383	2459	5^+	4^+	0.49(5)
2166.4 (5)	11 (1)	12 (2)	3620	1454	4^+	2^+	1.18(51)
2504.2 (13)	5 (2)	6 (1)	4964	2459	(5)	4^+	1.18(51)
2653.7 (12)	3 (1)	3 (1)	4108	1454	4	2^+	0.82(29)
2668.6 (10)	16 (3)	14 (2)	5128	2459	6^+	4^+	1.06(9)
2926.5 (15)	3 (1)	2 (1)	5386	2459	(5,6)	4^+	0.90(27)
3626.2 (16)		1 (1)	6085	2459	(6)	4^+	0.86(27)

Hatsukawa study [32]. It is consistent with an $M1/E2$ character from its DCO ratio of 0.30 ± 0.01, but there are no other transitions observed decaying from this state to confirm the validity of the DCO gate. However, an $M1/E2$ assignment is favored over an $E2$ one due to the weak intensity, which suggests a nonyrast state. If the decaying level had a spin of $\frac{17}{2}$, it would constitute the yrast level at this spin, and might be expected to be more strongly populated. Also, if the state had a negative parity, an $E2$ transition feeding the 3016 keV, $\frac{11}{2}^-$ level would most likely be seen.

(xv) 5120 keV level. The DCO ratio of 1.02(4) for the 1039 keV transition suggests that this level is a $\frac{17}{2}^+$. This is in agreement with the 529 keV transition which feeds the 4590 keV level having an $E2$ characteristic DCO ratio of 0.94(10).

(xvi) 5138, 5703, and 6056 keV levels. The spin and parity assignments of the levels in the cascade built on the 4288 keV $\frac{13}{2}^-$ state cannot be made with confidence based on DCO ratios alone, leaving the levels connected by the 353, 565, and the 850 keV cascade unassigned. However, assignments may be tentatively made using an alternative suggestion. The value of 0.63 ± 0.10 for the 850 keV γ ray suggests an $E1$ transition, which would make the 5138 keV level a $\frac{15}{2}^+$. The 565 keV line has a large uncertainty in its ratio, but following the arguments laid out here, it has been tentatively assigned as a $J \rightarrow J$ transition. The 353 keV transition has a DCO value of 0.49 ± 0.11, indicating a $\Delta I = 1$ transition, which would lead to the 6056 keV level having an assignment of $\frac{17}{2}^+$. If the 1975 keV transition to the 4081 keV, yrast $I^\pi = \frac{13}{2}^+$ state is an $E2$ transition, the decaying state at 6056 keV would have $\frac{17}{2}^+$ I^π. The DCO ratio of this transition is undetermined as it is weakly populated. However, the energies of the γ-ray transitions below each state add up to 6056.1 ± 1.3 for the level decaying via the 1975 keV γ-ray, and 6055.6 ± 1.6 for the level decaying via the 353 keV γ-ray, and it is, therefore, suggested that the 1975 and the 353 keV transitions are parallel decays from the same 6056 keV level. Spin and parity assignments for the three

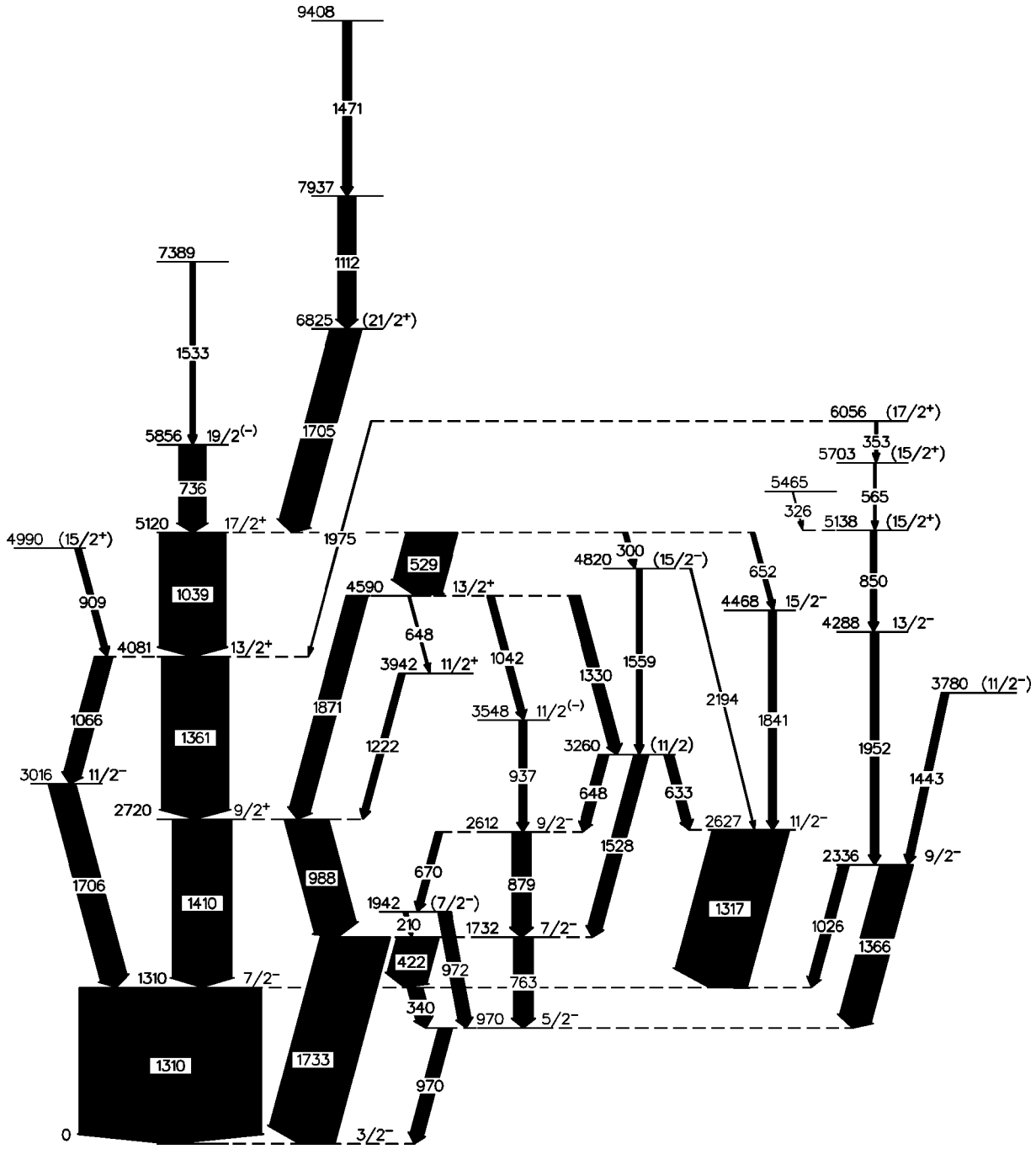

FIG. 10. Partial decay scheme for ^{61}Cu deduced in the present work.

transitions directly below this level are, thus, tentatively proposed on this basis. None of these transitions are reported by Hatsukawa in Ref. [32].

(xvii) 5856 keV level. The DCO ratio of the 736 keV line is 0.56(3), and this transition is accordingly assigned as a dipole and, tentatively, of an electric nature, making the 5856 keV level a $\frac{19}{2}^{(-)}$.

(xviii) 6825 keV level. The 1705 keV transition can be studied with the DCO method using the 1361 keV transition as a gate, thus avoiding the doublet problem. The outcome is a ratio of 1.18(3), which has been interpreted tentatively as an $E2$.

All other transitions in this data set, depopulating the states at 5465, 7389, 7937, and 9408 keV, had insufficient statistics to extract useful numbers from this method; they consequently remain unassigned. This does, however, constitute the first observation of these states and their place in the decay scheme is therefore significant.

B. ^{61}Zn

Prior to this study, states had been observed up to 4413 keV in ^{61}Zn following the light-ion reaction ^{58}Ni$(\alpha,n)^{61}$Zn [36–38], the heavy-ion fusion-evaporation reactions

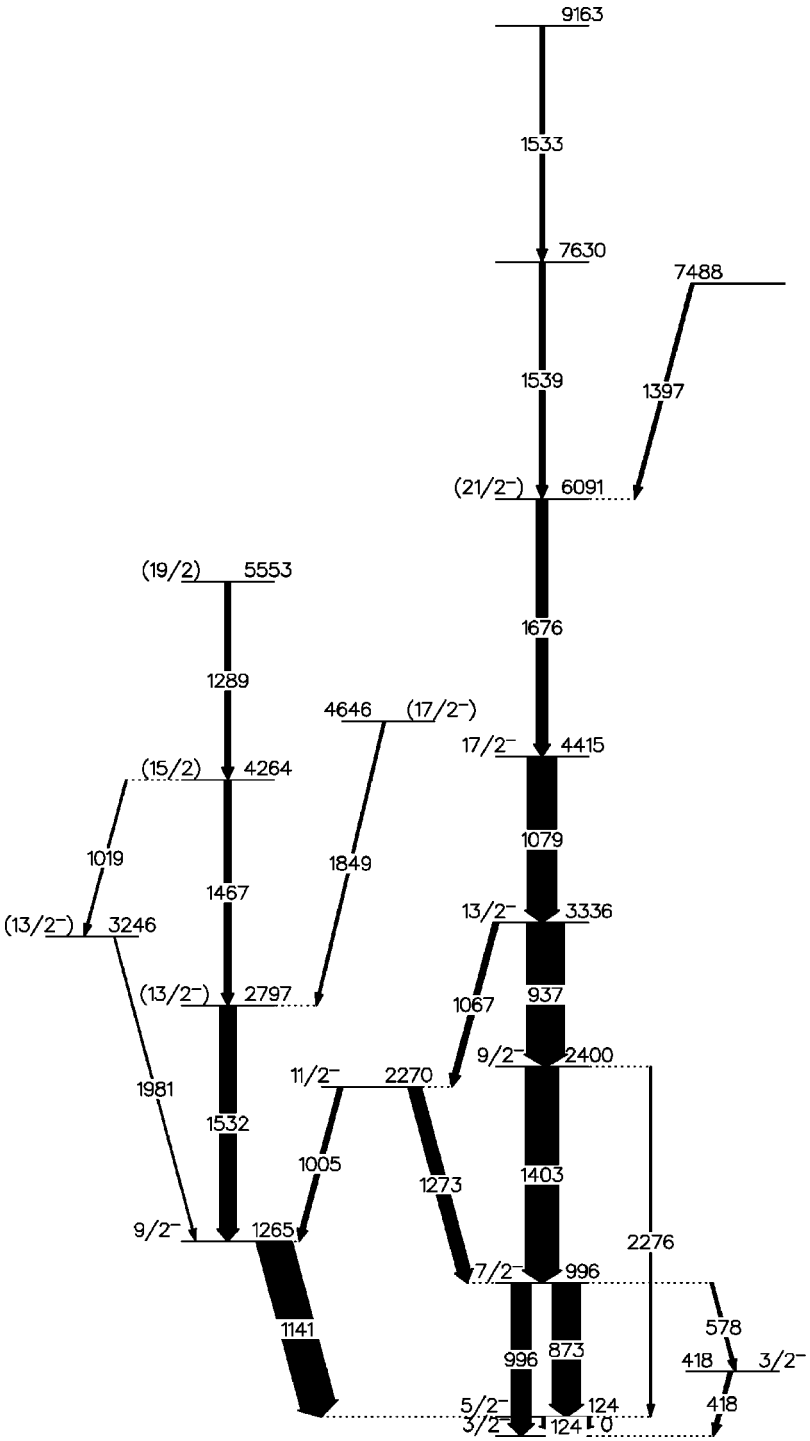

FIG. 11. Partial decay scheme for ^{61}Zn deduced in the present work.

^{58}Ni(^{6}Li,$p2n$)^{61}Zn, ^{54}Fe(^{10}B,$p2n$)^{61}Zn, and ^{40}Ca(^{24}Mg, $2pn$)^{61}Zn [36], and the particle transfer reactions ^{58}Ni(^{12}C,^{9}Be)^{61}Zn [52], and ^{58}Ni(^{6}Li,t)^{61}Zn [53]. All the near yrast energy level assignments made in earlier work are in agreement with the decay scheme derived from these data, except for the specific example of the 2400 keV level mentioned below. In the study by Schubank *et al.* [36], the low lying yrast and nonyrast levels were observed, including all the states identified in this work up to 3336 keV. As with the ^{61}Cu study, many of the nonyrast states previously identified are not observed in this work. For example, Schubank observed a $\frac{1}{2}^-$ state at 88 keV, a $\frac{5}{2}^-$ state at 755 keV, another $\frac{1}{2}^-$ level at 938 keV, a $\frac{3}{2}^-/\frac{5}{2}^-$ state at 1361 keV, and a $\frac{7}{2}^-$ level at 1402 keV, all of which are absent here. This work extends the near yrast data with eight new levels up to 9163 keV, and determines spins and parities of the previously observed levels at 2270, 2400, 3336, and 4415 keV.

The ground-state spin and parity of ^{61}Zn was theoretically predicted to be $\frac{3}{2}^-$ by Webber *et al.* [52] and Sandhu [54], and confirmed experimentally in β decay studies by Dulfer *et al.* [55] and Hoffman and Sarantites [56].

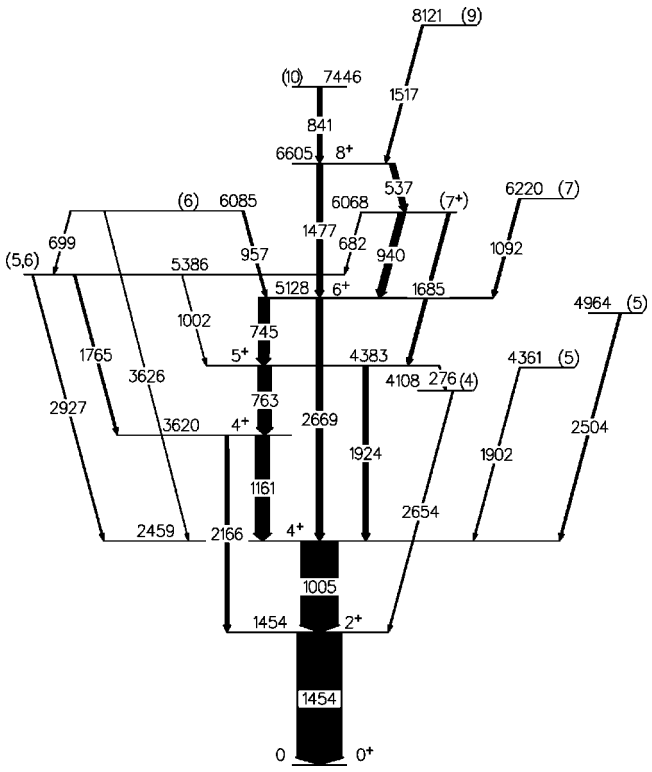

FIG. 12. Partial decay scheme for ^{58}Ni deduced in this work.

(i) 2270 keV level. The current analysis confirms the tentatively made $\frac{11}{2}^-$ assignment for this level [36] from the DCO ratios of 0.51(17) for the 1005 keV $M1/E2$ transition, and 1.25(33) for the 1273 keV $E2$ transition.

(ii) 2400 keV level. The present analysis also indicates a spin/parity assignment for this level of $\frac{9}{2}^-$ rather than $\frac{11}{2}^-$ as published in Ref. [36]. This statement is qualified by the DCO ratios of not only the 1403 keV transition, but also the assignments of the 1265, 2270, and 3336 keV levels and the decays into and out of these states.

(iii) 2797 keV level. This level is assigned a spin $\frac{13}{2}$ on the basis of the DCO ratio of the 1532 keV transition, being 1.26(17), but this is only a tentative assignment and this could conceivably be a $\frac{11}{2}$ state.

(iv) 3246 keV level. The spin of this level cannot be determined by the DCO method from these data with any confidence due to the large error on the ratio for the 1981 keV transition ratio. However, it could be either $\frac{11}{2}$ or $\frac{13}{2}$, the latter being tentatively preferred from the DCO analysis. The probable negative parity is due to the difficulty in generating positive parity states from the available orbital.

(v) 3336 keV level. The DCO ratio of 1.03(7) for the 937 keV transition to the 2400 keV $\frac{9}{2}^-$ state allows a $\frac{13}{2}^-$ assignment with confidence.

(vi) 4264 keV level. This level has a tentatively assigned spin of $\frac{15}{2}$ from the DCO ratio for the 1467 keV transition depopulating it. If the level had a spin/parity of $\frac{13}{2}^-$, one might expect a stretched $E2$ transition to feed the 2400 keV $\frac{9}{2}^-$ state, and the nonobservation of this transition is consistent with the spin assignment shown.

(vii) 4415 keV level. The DCO ratio for the 1079 keV transition feeding out of this state is 1.03(25) which, despite the fairly large errors, is indicative of an $E2$ transition.

(viii) 4646 keV level. With a DCO ratio suggestive of an $E2$ transition for the 1849 keV, this level has been only tentatively assigned due to the low statistics.

(ix) 5553 keV level. Although the assignment of the 1289 keV transition is made with reasonable confidence as an $E2$, the spin of the lower state is uncertain, necessitating a tentative assignment for this level.

(x) 6091 keV level. This level has been tentatively assigned with the 1676 keV transition having a DCO ratio consistent with an $E2$.

It should be noted that a 755 keV transition is identified in the ^{61}Zn id-spectrum (Fig. 5), in agreement with one seen by Schubank [36] to decay from a 755 keV $\frac{5}{2}^-$ level to the $\frac{3}{2}^-$ ground state. However, the transition could not be linked with the rest of the decay scheme. No spin assignments could be made for the other three newly discovered states in the decay scheme due to poor statistics.

C. ^{58}Ni

While there has been considerable study of the low spin and nonyrast levels in this nucleus with light-ion induced reactions [9–13], the data on near yrast higher spin states are limited to states up to 5128 keV, plus one 537 keV transition depopulating a state of excitation energy 5662 keV and a tentative spin of 7 [40,41]. The present results extend the level scheme of ^{58}Ni up to an excitation energy of 8121 keV, and propose a new assignment for the 537 keV transition to depopulate the 6605 keV state. Seven other previously unreported states are also observed, and spins and parities are determined for four previously observed levels. Table III summarizes the information obtained for the transitions in ^{58}Ni. The spin and parity assignments for the previously unreported levels are discussed individually below.

(i) 4108 keV level. This level decays to the yrast 2^+ state at 1454 keV and is populated directly from the 5^+ level at 4383 keV. Thus, spin assignments can be restricted to 3 or 4, with $4\hbar$ favored on the basis of the population of near yrast states, as a spin $3\hbar$ assignment for this state would make it highly nonyrast. This level has been tentatively reported in (p,p') and $(p,p'\gamma)$ reactions with a spin assignment of 2^+ [57], which is unlikely in view of the decays observed here.

(ii) 4964 keV level. By decay arguments, the possible assignments for this level are 4^+, $5^\pm$, and 6^+. A nonyrast 4^+ state is unlikely, in light of the nonobservation of the previously reported low lying nonyrast 4^+ states at 4405 and 4755 keV [57]. A 6^+ assignment would make this state the yrast level for this spin, yet the relatively weak intensity of the 2504 keV transition, which links this state to the yrast 4^+ state at 2459 keV, does not support this argument. Therefore, a spin $5\hbar$ assignment is preferred. Unfortunately, the lack of statistics in the angular distribution and DCO data make it impossible to discriminate between a pure dipole and a mixed $E2/M1$ transition, and the parity of this state could not be determined.

(iii) 5386 keV level. Since this state decays to the levels at 2459, 3620, and 4383 keV, which have been assigned spins and parities 4^+, 4^+, and 5^+, respectively [57], possible quantum numbers can be restricted to $4^{\pm}$, $5^{\pm}$, or 6^+. A 4^+ assignment can be discounted through (1) the lack of an observed decay to the yrast 2^+ state at 1454 keV and (2) the highly nonyrast nature of such a state. The measured DCO ratio for the 1765 keV transition to the 4^+ state at 3620 keV of 0.50(0.16) suggests a $\Delta I=1$ decay. Therefore, a spin 5 assignment for the 5386 keV state is preferred, although a spin 6 assignment is possible. Unfortunately, the parity of this state could not be determined.

(iv) 6068 keV level. The observed decays from this state are via the 682 keV transition to the spin (5,6) state at 5386 keV, the 940 keV transition to the 6^+ level at 5128 keV, and the 1685 keV decay to the yrast 5^+ state at 4383 keV. A 6^+ assignment appears unlikely in view of the lack of an observed decay to the yrast 4^+ state, while a 7^- assignment can be ruled out by the observed decay to the yrast 5^+ state. Thus, the spin/parity assignment for this state can be restricted to 6^- or 7^+, with the higher value preferred on the basis of yrast feeding and intensity considerations.

(v) 6085 keV level. The observed decay from this level to the yrast 4^+ state at 2459 keV, coupled with the rather high excitation energy strongly, suggests a 6^+ assignment.

(vi) 6220 keV level. The tentative spin $7\hbar$ assignment for this level comes from the measured DCO value of 0.67 ± 0.23 for the 1092 keV γ ray. While, in principle, a spin $8\hbar$ assignment is also possible, the intensity of the 1092 keV decay is smaller than that of the 1477 keV line representing the decay from the 6605 keV 8^+ state, and a spin 7 assignment is preferred from yrast feeding arguments.

(vii) 6605 keV level. The observed decays to the yrast 6^+ and (7^+) states via the 1477 and 537 keV transitions, respectively, and the intense nature of these transitions, together with the measured DCO ratio, are consistent with an assignment of 8^+ for this state.

(viii) 7446 keV. The measured DCO ratio for the 841 keV transition, which links this state to the 8^+ state at 6605 keV, is indicative of a 10^+ assignment. While a spin $9\hbar$ cannot be conclusively ruled out, the higher spin assignment is preferred in view of the absence of any competing decay to the spin $(7)\hbar$ states at 6068 and 6220 keV.

(ix) 8121 keV level. This state is observed to decay to the yrast 8^+ level at 6605 keV via the 1517 line. The measured DCO ratio of 0.61 ± 0.12 supports a $\Delta I=1$ character and thus a spin assignment of $9\hbar$ for this state.

IV. SHELL MODEL COMPARISON AND DISCUSSION

Shell model calculations have been performed for ^{61}Cu, ^{61}Zn, and ^{58}Ni using a model space basis restricted to the $f_{5/2}$,$p_{3/2}$,$p_{1/2}$, and $g_{9/2}$ orbitals (henceforth called fpg-shell calculations). To derive the effective shell-model interaction, a perturbative many-body scheme starting with the free nucleon-nucleon interaction was used, as described in Ref. [58]. The bare nucleon-nucleon interaction used was the charge-dependent meson-exchange model of Machleidt and co-workers [59], the so-called CD-Bonn model. The model assumes a closed $^{56}_{28}\mathrm{Ni}_{28}$ core and does not allow for core breaking. For the protons, the single-particle energies of these active orbitals were calculated relative to the lowest $p_{3/2}$ state, and found to be 1.04 MeV for the degenerate $f_{5/2}$ and $p_{1/2}$ levels and 3.51 MeV for the $g_{9/2}$ orbital. The calculated energies for the neutron single-particle orbits, relative to the $p_{3/2}$ orbital, were 0.77 MeV for the $f_{5/2}$ level, 1.11 MeV for the $p_{1/2}$ state, and 3.70 MeV for the $g_{9/2}$ orbital.

A further calculation was performed for ^{58}Ni using the OXBASH code [60]. The two-body matrix elements were taken from the work of Gloeckner [61] and include no contribution from core excitation. This calculation used a $^{40}_{20}\mathrm{Ca}_{20}$ core, allowing promotions from the $f_{7/2}$ orbital, as well as maintaining excitations into the $f_{5/2}$, $p_{3/2}$, and $p_{1/2}$ orbitals (henceforth called full fp-shell calculation). In order to keep the calculation size manageable, it did not allow excitations into the $g_{9/2}$ state. The calculated energies for the neutron single-particle orbits, relative to the $f_{7/2}$ state, were 1.9 MeV for the $p_{3/2}$ orbital, 6.9 MeV for the $f_{5/2}$ orbital, and 3.8 MeV for the $p_{1/2}$ orbital.

A. ^{61}Cu shell model

For $^{61}_{29}\mathrm{Cu}_{32}$, the fpg-shell model space has four valence neutrons and one valence proton in the four active orbitals, and the maximum angular momentum that can be generated is $(\nu g_{9/2})^3_{21/2^+}\otimes(\nu f_{5/2})^1_{5/2^-}\otimes(\pi g_{9/2})^1_{9/2^+}=\frac{35}{2}^-\hbar$. The results of this calculation are compared with the experimental levels in Fig. 13.

While the calculation has not been used to unambiguously assign spins or parities, it has been useful in inferring probable assignments, or in supporting the validity of claims made from the DCO data or intensities.

The first $\frac{5}{2}^-$ state at 970 keV is well reproduced, but the $\frac{7}{2}^-$ level at 1310 keV is too high by $\sim$400 keV. This may suggest that excitation from the $f_{7/2}$ orbital in the ^{56}Ni core is important. The yrast $\frac{9}{2}^+$ state is also calculated too high by $\sim$800 keV, and since the $g_{9/2}$ intruder orbital has positive parity, it may be that it is not correctly modeled. However, the higher spin, positive parity, yrast experimental levels, namely, the $\frac{13}{2}^+$ and the $\frac{17}{2}^+$, are quite well reproduced by the calculation. In contrast, the calculated high spin negative parity states, namely, the $\frac{15}{2}^-$ and the $\frac{19}{2}^-$ are, in general, too high.

The 1942 keV level is tentatively assigned as a $\frac{7}{2}^-$ state on the basis of DCO ratios and intensity arguments, although a $\frac{9}{2}$ assignment is possible (see Sec. III A). This would make it the third lowest energy $\frac{7}{2}$ level, i.e., third yrast, compared to being the yrast $\frac{9}{2}$ level. The experimental value agrees much more closely with the negative parity calculations than the positive parity, and the third yrast $\frac{7}{2}^-$ theoretical state at 2566 keV is within 220 keV of the theoretical yrast state with the alternative $\frac{9}{2}$ spin, so this tentative assignment is theoretically valid.

The 4990 keV level matches closely with a $\frac{15}{2}^+$ state predicted at 4920 keV, consistent with the argument made earlier regarding such an assignment from its intensity (see Sec. III A). The 5138 keV level also matches the calculation bet-

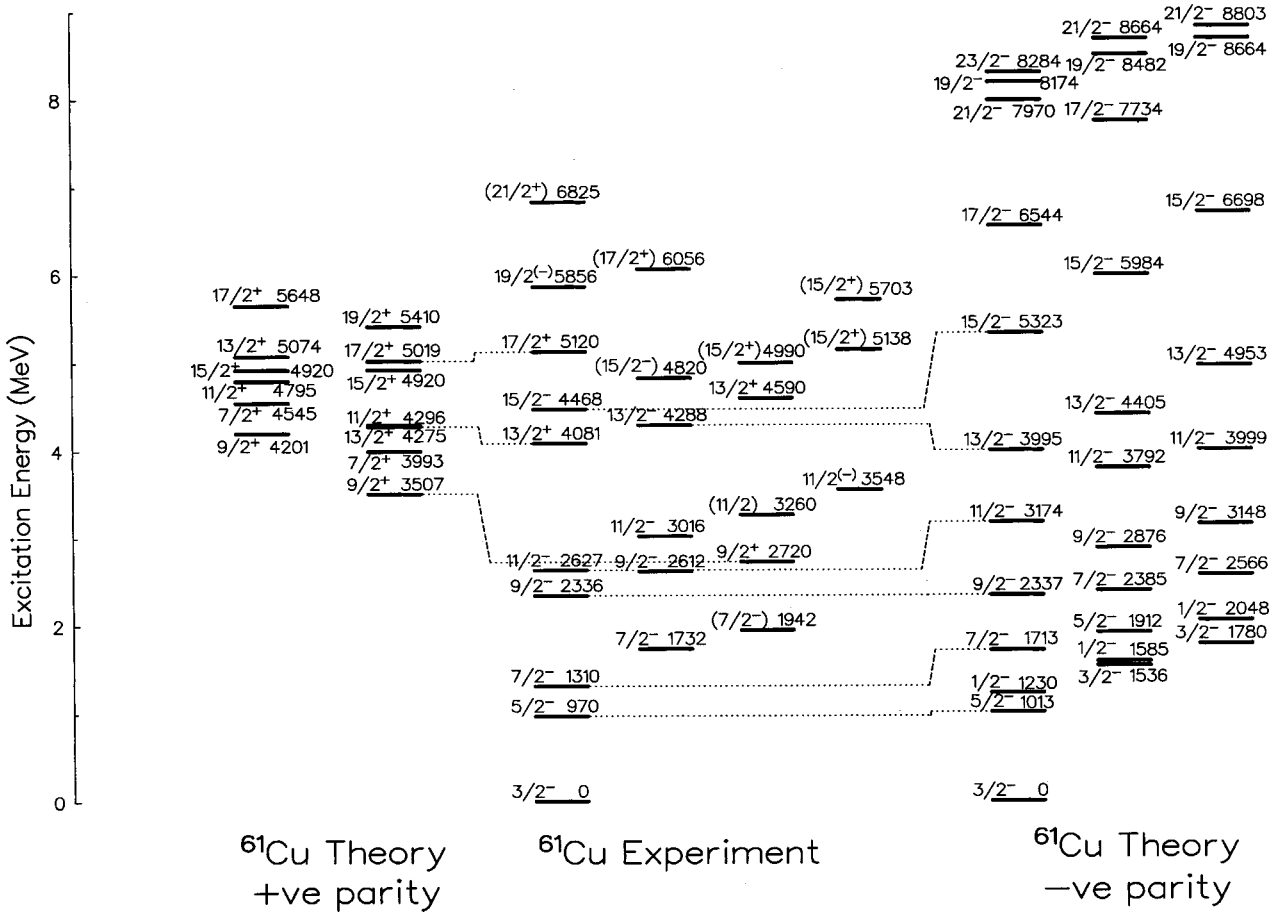

FIG. 13. Comparison of experimental data and fpg-shell theoretical calculations for ^{61}Cu. The highly nonyrast calculated levels are not shown.

ter as a $\frac{15}{2}^+$ state, in agreement with the suggestion that the 850 keV transition is of an $E1$ character. Indeed, all the states which decay into this level agree well with calculated values, which concur with the suggestion that the 6056 keV level at the top of this cascade is a $\frac{17}{2}^+$ state, and that this level also depopulates via the 1975 keV transition (see Sec. III A).

B. ^{61}Zn shell model

This fpg model space leaves three valence neutrons and two valence protons in the four active orbitals and so the maximum angular momentum this basis can generate is $(\nu g_{9/2})^2_{16/2^+} \otimes (\nu f_{5/2})^1_{5/2^-} \otimes (\pi g_{9/2})^2_{16/2^+} = \frac{37}{2}^- \hbar$. The results of this calculation are compared with the experimental levels in Fig. 14. Only negative parity states are produced by the calculation.

The degree of agreement between experimental and theoretical states at low energies is not as good as for ^{61}Cu. The first excited yrast state at 124 keV is predicted to be 807 keV higher than it is observed, and it was the first $\frac{5}{2}^-$ state which was calculated most accurately in the case of this same fpg-shell calculation for ^{61}Cu.

Although all the yrast states up to spin $\frac{17}{2}$ are calculated too high in energy, the energy spacing and the level ordering is correctly predicted. This gives some confidence in the spin assignments made from DCO and other arguments in Sec. III B.

The 5553 keV is most accurately correlated to the calculated $\frac{15}{2}^-$ state. Despite the preferential population of yrast or near yrast states in this type of reaction, this assignment is not unreasonable since the state is seen to decay only to the 4264 keV level in this data set. The experimental assignment of this level is based on that of the 2797 keV state being a $\frac{13}{2}$, but as described in Sec. III B, this is tentative, and could certainly be $\frac{11}{2}$. This would mean the 4264 keV level is a $\frac{13}{2}$, and given that the DCO ratio of 1.04(18) for the 1289 keV transition depopulating the 5553 keV state need not necessarily mean it is a stretched E2 due to the errors, this level could thus have a $\frac{15}{2}$ spin in close agreement with the calculation. Given the tenuous agreement between experiment and calculation for the other states, this is simply noted in the text, and the final assignment is made based on the arguments made in Sec. III B.

C. ^{58}Ni shell model

In the fpg-shell calculation, the model space leaves two valence neutrons outside the ^{56}Ni core, with excitations into the four active orbitals able to generate a maximum spin of $(\frac{9}{2})^2_{8+} = 8^+ \hbar$. Note that states are observed up to a tentative

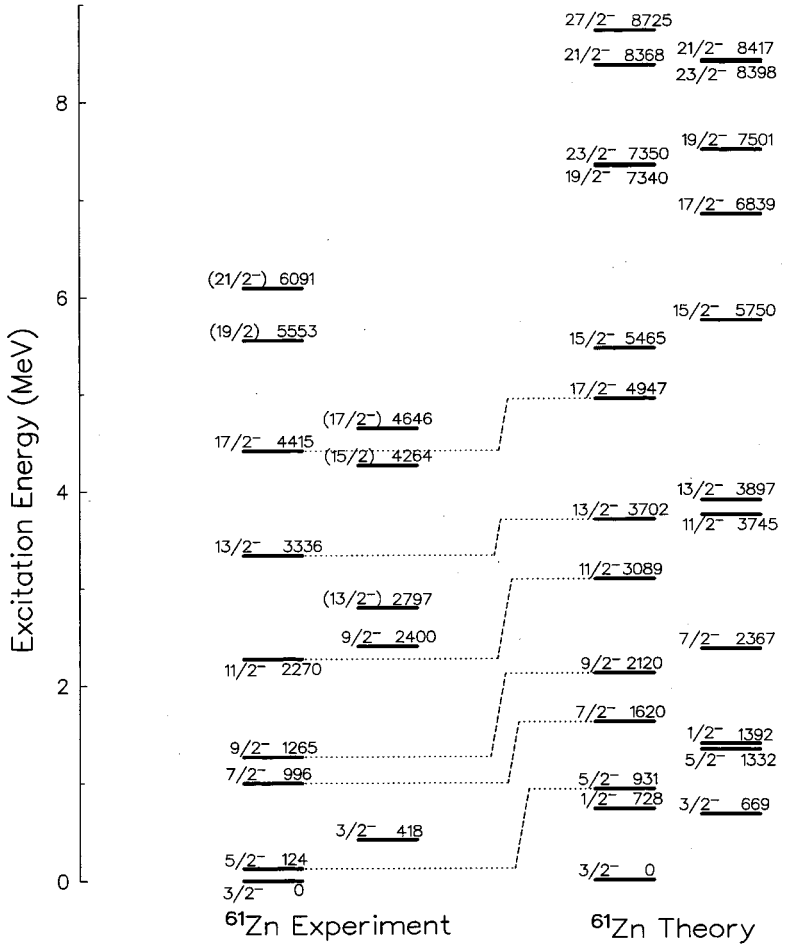

FIG. 14. Comparison of experimental data and fpg-shell theoretical calculations for ^{61}Zn. The highly nonyrast calculated levels are not shown.

10 $\hbar$ in the current work, and thus some degree of breaking of the $N=Z=28$ core must have occurred. With this restricted model space, states of spin/parity 5^+,7^+, or 9^+, and above cannot be generated since we only have neutrons and, hence, such combinations are Pauli forbidden. The full fp-shell calculation has 18 valence particles, 8 protons, and 10 neutrons, in the four active orbitals, and does include core breaking, so the higher spin states are feasible with this configuration.

The results of both of these calculations are compared with the experimental levels in Fig. 15 for positive and negative parity, separately. There are no negative parity states for the full fp-shell calculation as the positive parity $g_{9/2}$ orbital is blocked, and there are always an even number of valence particles.

The negative parity states in the fpg-shell calculation are relatively high in excitation energy due to the high intrinsic energy of the $g_{9/2}$ orbital.

The first 0^+, 2^+, and 4^+ states are well reproduced in both the fpg-shell and the full fp-shell calculations. The 6^+ and 8^+ are much too high in excitation energy from the fpg-shell calculation. There is also no 5^+, 7^+, or 9^+ state produced in this calculation. These levels are, however, all well reproduced by the full fp-shell calculation, which predicts the positive parity states fairly closely up to 8^+, including the tentatively assigned (7^+) level at 6068 keV. The high energy $6^+ \rightarrow 4^+$ transition of 2669 keV is predicted by the full fp-shell calculation (which includes core breaking), but which is not reproduced by the fpg-shell calculation (which has no core breaking). It is therefore considered to be a signature of breaking of the ^{56}Ni core, which becomes important above $\sim$4 MeV excitation energy. The spin and parity of the 7446 keV level could not be determined from the calculation since no states higher than spin $8\hbar$ were calculated.

V. SUMMARY AND CONCLUSIONS

In summary, the high spin states of the nuclei ^{58}Ni, ^{61}Cu, and ^{61}Zn have been studied with the AYEBALL+FMA configuration, identifying previously unobserved states up to excitation energies of 8121 keV, 9408 keV, and 9163 keV, respectively. The nuclei of interest were populated following the fusion evaporation reaction ^{24}Mg+^{40}Ca. The mass and charge of the recoiling nuclei were identified using the FMA, with the Z determined using an energy loss signal from the split anode ion chamber at the focal plane of the instrument. This allowed excellent separation of γ-ray transitions associated with the nuclei of interest. From the observed decays of the states, and using angular information (from mass gated γ-singles data) and DCO ratios (from the backed target γ-γ coincidence data), it was possible to assign spins and parities

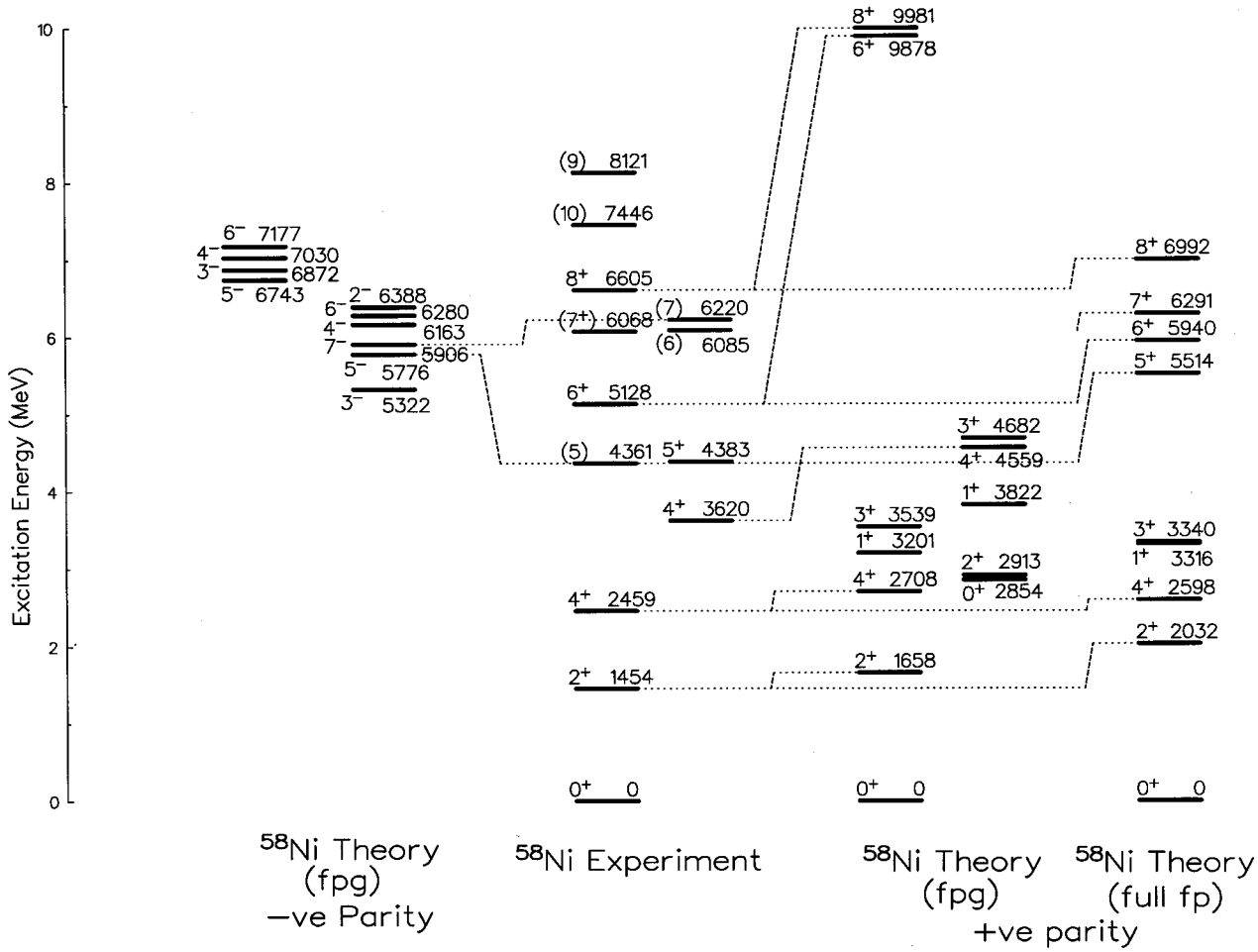

FIG. 15. Comparison of experimental data and both fpg-shell and full fp-shell theoretical calculations for ^{58}Ni. The highly nonyrast calculated levels are not shown.

to most of the states observed.

The resulting level schemes have been compared with shell model calculations using both a simple fpg basis with no core breaking, and a full fp basis which allowed no excitations into the $g_{9/2}$ orbital. In general, reasonable agreement has been obtained at low excitation energy between experimental results and simple fpg-shell model calculations, suggesting that the low-lying yrast excited states in the nuclei around the ^{56}Ni core correspond predominantly to valence particle excitations into the $f_{5/2}$, $p_{3/2}$, and $p_{1/2}$ orbitals. In ^{61}Cu and ^{61}Zn, higher energy and spin states are fairly well accounted for by allowing only excitations into the positive parity $g_{9/2}$ orbital, with no core breaking. However, the experimental data for ^{58}Ni above the first 4^+ level become significantly closer to the full fp-shell calculation, which allows for promotion from the $f_{7/2}$ orbital in the ^{56}Ni core, rather than the fpg-shell calculation, which allows only excitation into the $g_{9/2}$ orbital. The large energy gap often associated with the breaking of the core is seen as the 2669 keV $6^+ \rightarrow 4^+$ transition in this nucleus, which is mimicked by the full fp-shell calculation. This suggests that in ^{58}Ni, core breaking becomes the dominant method of angular-momentum generation at around 4 MeV and $\sim 5\hbar$.

ACKNOWLEDGMENTS

This work has been supported by the Engineering and Physical Sciences Research Council (EPSRC) (U.K.), and by the U.S. Department of Energy, Nuclear Physics Division under Contract No. W-31-109-ENG-38. S.M.V. acknowledges the support of the EPSRC.

[1] M. Lipoglavsek *et al.*, Phys. Rev. Lett. **76**, 888 (1996).
[2] J. Cederkäll *et al.*, Phys. Rev. C **53**, 1955 (1996).
[3] H. Grawe *et al.*, Z. Phys. A **358**, 185 (1997).
[4] M. Gorska *et al.*, Phys. Rev. C **58**, 108 (1998).
[5] H. Grawe, M. Górska, M. Lipoglavsek, J. Nyberg, R. Grzywacz, M. Lewitowicz, K. Rykaczewski, K.H. Maier, and R. Schubart, Prog. Nucl. Part. Phys. (to be published).
[6] D. Rudolph *et al.*, Nucl. Phys. **A630**, 417c (1998).
[7] D. Rudolph *et al.*, Z. Phys. A **358**, 379 (1997).
[8] M. Ramdhane *et al.*, Phys. Lett. B **432**, 22 (1998).

[9] O.N. Jarvis, Nucl. Phys. **A102**, 625 (1967).
[10] T. Suehro, Phys. Lett. **33B**, 468 (1970).
[11] D. Evers, Nucl. Phys. **A198**, 268 (1972).
[12] M.C. Mallet-Lemaire, Phys. Lett. **53B**, 279 (1975).
[13] T. Suehro, Phys. Lett. **53B**, 449 (1975).
[14] M.G. Saint-Laurent, Sl. Cavallaro, M.L. Sperduto, B. Delaunay, J. Delaunay, and H. Dumont, Z. Phys. A **334**, 365 (1989).
[15] W. Nazarewicz, in *Contemporary Topics in Nuclear Structure Physics*, edited by R.F. Casten *et al.* (World Scientific, Hong Kong, 1988), p. 467.
[16] I. Ragnarsson, Proceedings of the Workshop on the Science of Intense Radioactive Ion Beams, Los Alamos, NM, edited by J.B. McClelland and D.J. Vieria, LANL Report No. 11964 (1990), p. 199.
[17] C.E. Svensson *et al.*, Phys. Rev. Lett. **79**, 1233 (1997).
[18] C.E. Svensson *et al.*, Phys. Rev. Lett. **80**, 2558 (1998).
[19] D. Rudolph *et al.*, Phys. Rev. Lett. **80**, 3018 (1998).
[20] D. Rudolph (private communication).
[21] S.M. Vincent *et al.*, J. Phys. G **25**, 941 (1999).
[22] M.P. Carpenter, Z. Phys. A **358**, 261 (1997).
[23] P.J. Nolan, D.W. Gifford, and P.J. Twin, Nucl. Instrum. Methods Phys. Res. A **236**, 95 (1985).
[24] J. Simpson, M. Bates, C. Brookes, and P.J. Nolan, Instrum. Methods Phys. Res. A **269**, 209 (1988).
[25] C.W. Beausang *et al.*, Nucl. Instrum. Methods Phys. Res. A **313**, 37 (1992).
[26] A.M. Baxter, T.L. Khoo, M.E. Bleich, M.P. Carpenter, I. Ahmad, R.V.F. Janssens, E.F. Moore, I.G. Bearden, J.R. Beene, and I.Y. Lee, Nucl. Instrum. Methods Phys. Res. A **317**, 101 (1992).
[27] C.N. Davids, B.B. Back, K. Bindra, D.J. Henderson, W. Kutschera, T. Lauritsen, Y. Nagame, P. Sugathan, A.V. Ramayya, and W.B. Walters, Nucl. Instrum. Methods Phys. Res. B **70**, 358 (1992).
[28] A. Galindo-Uribarri, D. Ward, G.C. Ball, V.P. Janzen, D.C. Radford, I. Ragnarsson, D. Headly, Phys. Lett. B **422**, 45 (1998).
[29] K. Furutaka, T. Hayakawa, H. Nakada, Y. Hatsukawa, M. Kidera, M. Oshima, S. Mitarai, H. Kusakari, T. Komatsubara, M. Matsuda, and K. Furuno, Z. Phys. A **358**, 279 (1997).
[30] G.F. Knoll, *Radiation Detection and Measurement* (J. Wiley, New York, 1989).
[31] S.M. Vincent, Ph.D. thesis, University of Surrey, 1998 (unpublished).
[32] Y. Hatsukawa *et al.*, Z. Phys. A **359**, 3 (1997).
[33] J.H. Barker, D.G. Sarantites, Ö. Skeppstedt, E. Wallander, G. Alenius, and S.E. Arnell, Phys. Rev. C **18**, 119 (1978).
[34] D.G. Sarantites, J.H. Barker, N.H. Lu, E.J. Hoffman, and D.M. Van Patter, Phys. Rev. C **8**, 629 (1973).
[35] C.E. Svensson *et al.*, Nucl. Instrum. Methods Phys. Res. A **396**, 228 (1997).
[36] R.B. Schubank, J.A. Cameron, and V.P. Janzen, Phys. Rev. C **40**, 2310 (1989).
[37] J.M. Thirion, G. Chouraqui, Th. Muller, and M. Port, Z. Phys. A **317**, 329 (1984).
[38] P.J. Smith, L.P. Ekström, F. Kearns, P.J. Twin, and N.J. Ward, J. Phys. G **8**, 281 (1982).
[39] K. Spohr *et al.*, Acta Phys. Pol. B **26**, 297 (1995).
[40] R. Ballini, N. Bendjaballah, J. Delaunay, J.P. Fouan, and W. Tokarevski, Nucl. Phys. **A258**, 388 (1976).
[41] G.J. Smith, R.O. Sayer, R.L. Robinson, and W.T. Milner, Oak Ridge National Laboratory Annual Progress Report, ORNL 4973, 1974, p. 115.
[42] K.S. Krane, R.M. Steffen, and R.M. Wheeler, Nucl. Data Tables **11**, 351 (1973).
[43] A. Krämer-Flecken, T. Morek, R.M. Lieder, W. Gast, G. Hebbinghaus, H.M. Jäger, and W. Urban, Nucl. Instrum. Methods Phys. Res. A **275**, 333 (1989).
[44] C. Bargholtz and P.E. Tegnér, Nucl. Instrum. Methods Phys. Res. A **256**, 513 (1987).
[45] S.M. Vincent *et al.*, Phys. Lett. B **437**, 264 (1998).
[46] P.J. Nolan and J.F. Sharpey-Schafer, Rep. Prog. Part. Nucl. Sci. **42**, 1 (1979).
[47] P.H. Regan, J.W. Arrison, U.J. Hüttmeier, and D.P. Balamuth, Phys. Rev. C **54**, 1084 (1996).
[48] J. Sziklai, T. Vaas, J.A. Cameron, and I.M. Szöghy, Phys. Rev. C **41**, 849 (1990).
[49] C.I.W. Tingwell, V.Y. Hansper, S.G. Tims, A.F. Scott, A.J. Morton, and D.G. Sargood, Nucl. Phys. **A496**, 127 (1989).
[50] H.M. Sen Gupta, J.B.A. England, F. Khazaie, E.M.E. Rawas, and G.T.A. Squier, Nucl. Phys. **A512**, 97 (1990).
[51] A.K. Singh and G. Gangopadhyay, Phys. Rev. C **55**, 2734 (1997).
[52] D.J. Webber, G.M. Crawley, W. Benenson, E. Kashy, and H. Nann, Nucl. Phys. **A313**, 385 (1979).
[53] C.W. Woods, N. Stein, and J.W. Sunier, Phys. Rev. C **17**, 66 (1979).
[54] T.S. Sandhu and M.L. Rustgi, Phys. Rev. C **12**, 666 (1975).
[55] G.H. Dulfer, B.O. ten Brink, T.J. Ketel, A.W.B. Kalshoven, and H. Vereul, Z. Phys. **251**, 416 (1972).
[56] E.J. Hoffman and D.G. Sarantites, Nucl. Phys. **A157**, 584 (1970).
[57] L.K. Peker, Nucl. Data Sheets **61**, 189 (1990).
[58] M. Hjorth-Jensen, T.T.S. Kuo, and E. Osnes, Phys. Rep. **261**, 125 (1995).
[59] R. Machleidt, F. Sammarruca, and Y. Song, Phys. Rev. C **53**, 1483 (1996).
[60] B.A. Brown, A. Etchegoyen, W.D.M. Rae, and N.S. Godwin (unpublished).
[61] D.H. Gloeckner, Nucl. Phys. **A253**, 301 (1975).